JOURNAL OF GEOPHYSICAL RESEARCH, VOL. 113, D16206, doi:10.1029/2007JD009607, 2008

Determination of index of refraction and size of supermicrometer particles from light scattering measurements at two angles

Trude Eidhammer,[1,2] Derek C. Montague,[2] and Terry Deshler[2]

Received 15 November 2007; revised 29 April 2008; accepted 29 May 2008; published 23 August 2008.

[1] A twin angle optical particle counter (TAOPC) that measures forward scattering at 40° and 74° was developed to determine the index of refraction of atmospheric particles. An error analysis indicates that measurement uncertainties for size at 40° are between 4 and 10% for particles >1.5 μm and between 5 and 15% at 74°. For the index of refraction determination, the measurement uncertainties lead to index of refraction uncertainties between 1 and 2.5%. The instrument was tested on nonabsorbing spherical particles of known composition and size in the laboratory. The majority of the estimated indices of refraction were within ±1% of the expected indices, and size determination was within acceptable error. The instrument was also tested on non-spherical absorbing particles to determine the complex index of refraction of ambient mineral dust particles collected in Laramie, Wyoming, in February 2006. The index of refraction was determined with the particle number ratio approach and was estimated to be in the range 1.60–1.67 for the real part and 0.009–0.0104 for the imaginary part. Simultaneously with the TAOPC measurements, particles were collected on polycarbonate filters for computer-controlled scanning electron microscopy (CCSEM) analysis. Index of refraction calculated from this analysis was in the range 1.61–1.66 for the real part and 0.008–0.012 for the imaginary part. Particles were also collected for longer periods on two different filter pack systems in February 2006. Estimates of index of refraction from these measurements compared well with the CCSEM analysis.

Citation: Eidhammer, T., D. C. Montague, and T. Deshler (2008), Determination of index of refraction and size of supermicrometer particles from light scattering measurements at two angles, *J. Geophys. Res.*, *113*, D16206, doi:10.1029/2007JD009607.

1. Introduction

[2] Aerosols directly affect radiation transfer in the atmosphere through scattering and absorption in both the short and long-wave region, and indirectly because of the effect of aerosols on cloud properties. Aerosol optical properties are influenced by the composition, concentration and size distribution of the particles. Optical particle counters (OPCs) are often used to measure aerosol size distributions and concentration; however, OPCs are sensitive to the optical size, and thus the shape and index of refraction of the particles, properties that are not easily determined. Most often it is assumed that the particles are spherical, so that the scattering theory by *Mie* [1908] can be used to relate measured scattering to particle size. In addition, for most OPCs, an index of refraction must be assumed for the size determination. By assuming an index of refraction different from the true index of refraction, the retrieved size distribution derived from the OPC measurements can be in error. Hence the true size distribution of aerosols hinges on knowing the index of refraction of the observed particles. OPCs that measure scattering at multiple angles have been developed, and these instruments can be utilized to determine particle size and index of refraction simultaneously. Several techniques have been developed for dual angle OPCs [*Baumgardner et al.*, 1996; *Zhao et al.*, 1997; *Szymanski et al.*, 2000; *Hu et al.*, 2006], multiangle OPCs [*Dick et al.*, 1994] or two-dimensional angular scattering pattern instruments [*Aptowicz et al.*, 2006]. Most techniques require extensive post-measurement analysis or consider individual particles. For absorbing particles there are several possible solutions for a complex index of refraction ($m = n - ik$) when only single particles are considered, because there are only two measurements (scattering at two angles), but three unknowns (size, and real and imaginary index of refraction). To address this difficulty *Hu et al.* [2006] developed a simple and fast technique to determine both the size distribution and average complex index of refraction of an aerosol sample simultaneously.

[3] Here laboratory and field measurements with a new twin angle OPC (TAOPC), which measures scattering at 40° and 74°, are presented. The laboratory measurements were carried out on particles of known size and index of refraction as a test of retrieving index of refraction of pure scattering particles. The field test was completed on mineral dust particles, which were measured for 2 hours with the

[1]Department of Atmospheric Science, Colorado State University, Ft. Collins, Colorado, USA.
[2]Department of Atmospheric Science, University of Wyoming, Laramie, Wyoming, USA.

0148-0227/08/2007JD009607$09.00

TAOPC in Laramie, Wyoming, a small urban mid continental North American location. For this test, the analytical technique developed by *Hu et al.* [2006] was used to determine the complex index of refraction. Simultaneously, particles were collected on three filter pack systems. Index of refraction can also be estimated on the basis of the composition found on the filters [*Ouimette and Flagan*, 1982; *Hasan and Dzubay*, 1983; *Stelson*, 1990]. The TAOPC and filter estimates are compared to each other and to previous measurements of tropospheric aerosol index of refraction.

2. Twin Angle OPC

[4] The TAOPC is based upon the University of Wyoming OPC (UWOPC) [*Rosen*, 1964; *Hofmann et al.*, 1975; *Hofmann and Deshler*, 1991; *Deshler et al.*, 2003a] which measures scattering at 40° for particle size determination. Measurements with the UWOPC are focused on the stratosphere, where the primary particles measured are sulfuric acid and water droplets or polar stratospheric cloud particles, which consist of ice, or nitric acid and water. These instruments have been used to find a correlation between ozone loss and volcanic aerosols [*Deshler et al.*, 1996], compared with satellite measurements [*Hervig et al.*, 1998], and compared with laser and lidar instruments to determine particle composition and refractive index [*Deshler et al.*, 2000]. Measurements with the UWOPC are regularly conducted in Laramie, Wyoming [*Deshler et al.*, 2003a] and McMurdo Station, Antarctica [*Adriani et al.*, 1995]. The instruments have also been used in Kiruna, Sweden [*Deshler et al.*, 2003b], Lauder, New Zealand [*Deshler et al.*, 1997], Darwin, Australia (2005) and Niamey, Niger (2006).

[5] Since the UWOPC only measures scattering at one angle, the index of refraction of the particles must be assumed. Routinely a value of 1.45 is assumed since this is in the midst of the narrow range of real indices of refraction assumed for sulfuric acid and water droplets [*Palmer and Williams*, 1975]. The small dependence of the index of refraction on temperature does not lead to large errors in size determination. For polar stratospheric cloud particles, however, an assumed index of refraction of 1.45 might lead to a 10% error in the size determination [*Deshler et al.*, 2000], indicating the importance of knowing the index of refraction of the particles measured.

[6] The main differences between the TAOPC and the UWOPC are the additions of measurements at a second angle, 74°, and a data acquisition system which provides single particle pulse height information. In contrast, the UWOPC measures particles greater than 12 pre-determined radii (>0.15 – 10.0 μm) and the numbers of particles counted in each bin are collected every 10 s. Thus the measured size distributions are integrations over 10 s. The data acquisition system used with the TAOPC collects and stores pulse shape and height for each particle passing the sensing volume. Thus particle size and index of refraction can be determined for each individual particle.

[7] The light source used in the TAOPC is white light from an incandescent lamp filament. Scattering by particles with size close to the wavelength of the light source develops resonance which causes oscillation in the counter response function for any OPC. To determine the size and index of refraction of particles, the counter response function must be monotonic with size, at a minimum of one angle. This can be obtained by including signals from multiple wavelengths, or by integrating the scattering over a large solid angle. Both these factors are true for the TAOPC. Generally white light counters are less sensitive than laser counters, but the counter response curves are more monotonic.

[8] Air is sampled by the TAOPC at a flow rate of 10 liters per minute (LPM). To avoid diffusion of the sample airflow, it is merged with clean sheath flow before the sample airflow reaches the illuminated region. The sheath flow has the same velocity as the sample airflow to ensure that particles are confined within the sample airflow and do not disperse. The sample airflow is in the transformation region between laminar and turbulent flow at air pressures greater than about 400 hPa. Loss of particles due to dispersion, however, is assumed to be minimal because the light sensing area is only ~4 mm from the end of the inlet, and therefore there is not significant time for dispersion of particles before they enter the sensing area.

[9] The white light is focused on the sample airflow with a condenser lens; particles in the airflow are illuminated by the focused light and scatter light in all directions. To eliminate regions of low or no illumination in the sample volume, the illuminated region is designed to exceed the sample volume. The inlet diameter in the TAOPC is ~3 mm, while the height of the illuminated volume is ~5 mm. Thus particles entering the illuminated region are well within the bounds of this region.

[10] In the horizontal direction, perpendicular to the sample airflow, the maximum light intensity is in the middle of the sample volume while the strength of the illumination is decreasing on both sides of the center. Therefore there may be some variations in the illumination of particles entering the illuminated region, depending on the location of the particles. However, measurements indicate that uneven illumination is a small factor in measurement error (section 3.2), and the decrease in the light intensity from the center of the illuminated region is assumed to be low. The intensity of the light in the vertical direction varies little. The filament itself is tightly coiled, with no open areas, leading to uniform illumination in the focused area.

[11] The light scattered from the particles is collected with photomultiplier tubes (PMTs), over 0.13 steradians for the PMTs centered at 40°, and 0.17 steradians for the PMT centered at 74°. Only a fraction of the photons hitting the PMTs cause signal multiplication. This percentage, called the quantum efficiency (*QE*), is dependent on the wavelength of incoming photons. The scattered light, as measured by the TAOPC after signal multiplication in the PMT is therefore a function of *QE* and the wavelength-dependent intensity of the light source. The maximum intensity of the scattered light measured is at ~0.52 μm, compared with ~0.9 μm for the incoming light, due to the *QE* of the PMT.

2.1. Sources of Measurement Uncertainties

[12] There are several sources for measurement error and uncertainties with the TAOPC: cosmic rays, coincidence, uneven illumination and statistical broadening in the PMT. To reduce noise and influences from cosmic rays, two PMTs

located at 40° are used and only pulses that are detected simultaneously by the two PMTs are accepted.

[13] If the number concentration of particles in a sample is too high, two or more particles can enter the sensing volume simultaneously leading to coincidence. The collective scattering from these particles is higher than from each individual particle, causing overestimation of size and underestimation of number concentration. For example, concentration loss of particles for a sample of 10 cm^{-3}, with the flow rate of 10 LPM and transit time of 50 μs in the TAOPC yields a loss of about 8% (equations (15–29) in the study by *Baron and Willeke* [2001]).

[14] The coincidence factor in the TAOPC, similar to the UWOPCs, can also be determined by comparing measurements conducted with UWOPCs and condensation nuclei (CN) counters simultaneously. The flow rate in the CN counter, developed at the University of Wyoming and used for stratospheric measurements [*Deshler et al.*, 2003a] is 1 LPM, and the particle inlet is 1 mm in diameter. This leads to a transit time of about 56 μs. With a concentration of 10 cm^{-3} (typical concentration of CN in the stratosphere), the loss due to coincidence in the CN counter is only 1% (compared to 8% in a UWOPC and the TAOPC). On several occasions, simultaneous measurements of PSCs with a UWOPC and a CN counter have shown that all CN particles have grown into polar stratospheric cloud particles [*Deshler et al.*, 2000, 2003b]. In these cases the concentration of particles >0.15 μm from UWOPC measurements matches the CN concentration of $\sim$10 cm^{-3}. Since the UWOPC and CN counter measure the same concentration [*Deshler et al.*, 2000, Figure 3b], the coincidence loss in the UWOPC (and TAOPC), as in the CN counter, can be assumed to be less than 1% for concentrations less than $\sim$10 cm^{-3}.

[15] Non-uniform illumination of particles can lead to under- or oversizing, which again leads to errors in concentration. The latter possibility can be checked through the same comparisons between the UWOPC and CN counters for concentration loss described in the previous paragraph. Since the light filament is tightly coiled, any eventual non-uniform illumination in the instruments would arise from less light at the edges of the illuminated region. The optical system in the CN counter is the same as in the UWOPC, thus the illuminated region is the same in both instruments. However, the inlet diameter of the CN counter is 1 mm while the inlet diameter of the UWOPC is 3 mm, leading to a smaller sampling volume in the CN counter, and thus less possibility of under-illumination of the aerosol sample. Since the concentration measured with a UWOPC and a CN counter in the example described above is the same for particles >0.15 μm, concentration uncertainties due to non-illumination problems with UWOPCs (and the TAOPC) can, in general, be assumed to be low. A second effect of undersizing is that the measured distribution of monodisperse particles may have a tail toward smaller sizes. Laboratory measurements, however, show that signals from monodisperse aerosols are close to normally distributed with only a small tail toward smaller sizes. This leads again to the conclusion that uncertainties due to non-uniform illumination are small in the TAOPC.

[16] The PMTs are the cause for the largest uncertainties in measured scattering with the TAOPC. The output signal from the PMT gives a Gaussian distribution for monodisperse particles primarily because of photoelectric pulse broadening in the PMT. The pulse broadening arises from the statistical nature of the photoelectric effect and secondary emission processes in the PMTs. *Miao* [2001], investigating the effect of photoelectric statistical broadening for the PMTs used in the UWOPCs, found that sizing errors were larger for small particles (low PMT signal) than for large particles. For the 40° PMT, errors are respectively 4, 8, and 40% for particles with radii of 2, 1, and 0.15 μm, the smallest size measurable. Similar relationships have also been observed by *Pinnick and Hofmann* [1973] and *Sugita et al.* [1999]. This point is considered again in section 3, which presents the current laboratory measurements.

[17] In addition to studying measurement uncertainties at 40°, *Miao* [2001] also studied the uncertainties arising from mounting the PMT at 74°. The results show that the measurement errors at 74° are larger than at 40°, because the scattered light intensity at 74° is relatively less than at 40°. To ensure a strong voltage signal from the scattered light at 74°, the signal gain in the PMT must be higher than at 40°. The increase in gain increases measured PMT distribution widths, which increases relative error since the counter response signal is relatively low at 74°. The effect of the pulse width broadening will be quantified after measurements in the laboratory are presented.

2.2. Counter Response Calculation, and Size and Index of Refraction Determination

[18] The counter response of both the TAOPC and UWOPC is dependent on the intensity and wavelength of the incoming light, the quantum efficiency of the PMT, the angles at which the PMT detects scattered light, the optical configuration of the instrument, and the size, index of refraction and shape of the particle. The geometry of the TAOPC (and UWOPC) optical system is shown in Figure 1. The angle between the axis of the focusing lens and the location of the PMT is denoted by Θ, where for the TAOPC, Θ is 40° and 74°. The scattered light is collected over the angles $\Theta \pm cl$. For the TAOPC, *cl* is 7.0° and 9.2° for the 40° and 74° PMT locations, respectively. The collection efficiency of the scattered light is described with the functions $CL(\theta)$ and $FL(\varphi, \theta)$ [*Pinnick*, 1972], where φ is the angle between the scattered light and the axis of the focusing lens. For the counter response calculation, $CL(\theta)$ is integrated over the angle $\Theta \pm cl$. The function $FL(\varphi, \theta)$ is, in addition to being a function of φ, also a function of the scattered light at angle θ. The latter angle is the true scattering angle measured, and it is the angle between the incoming light (coming from angles $\pm fl$ relative to the axis of the focusing lens) and the scattered light which is contained within $\Theta \pm cl$. For the TAOPC, *fl* is 9.6° at both the 40° and 74° PMT locations. The function $FL(\varphi, \theta)$ is integrated over all possible scattering angles, $\varphi \pm fl$ and $\Theta \pm cl$.

[19] By including the light collection efficiency functions, *FL* and *CL*, scattering efficiency terms ($\mathbf{i_1}$ and $\mathbf{i_2}$) calculated on the basis of Mie electromagnetic theory [*Mie*, 1908], the intensity of light (I_0), and the quantum efficiency (*QE*) of the PMTs, the counter response, *CR*, for a spherical particle

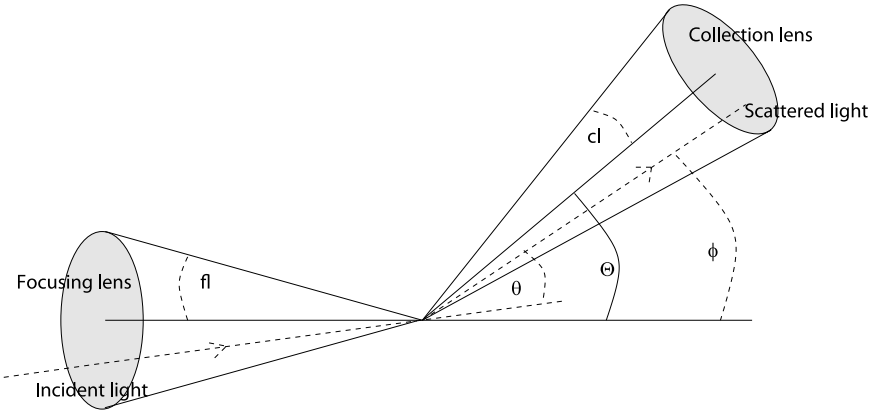

Figure 1. Optical geometry of the TAOPC.

in units of W is expressed with the triple integral [*Pinnick*, 1972; *Deshler et al.*, 2003a]:

$$CR = \int_{\Theta-cl}^{\Theta+cl} CL(\varphi)d\varphi \int_{\varphi-fl}^{\varphi+fl} FL(\varphi,\theta)d\theta \int_{0.3\,\mu m}^{0.7\,\mu m} \left(\frac{\lambda}{2\pi}\right)^2 \cdot \left[\frac{\mathbf{i_1}(x,m,\theta)+\mathbf{i_2}(x,m,\theta)}{2}\right] I_0(\lambda)QE(\lambda)d\lambda. \quad (1)$$

Here $x = 2\pi a/\lambda$ is the size parameter (a is particle radius), and m is the complex index of refraction. The scattering efficiency terms $\mathbf{i_1}$ and $\mathbf{i_2}$, I_0 and QE are all dependent on the wavelength of light. Since the TAOPC uses white light, the counter response must be integrated over the wavelength sensitivity range of the PMT (0.3 to 0.7 μm). Planck's function for a blackbody is used to calculate I_0, where the temperature is 3300 K. Example counter response curves are shown in Figure 2a for particles with different real indices of refraction (1.35 to 1.60 in steps of 0.05) at 40° and 74° angles. The imaginary index of refraction is zero. Measurements at 40° are used for size determination since the counter response is relatively monotonic with size at this angle. For determining index of refraction, the 74° angle is chosen because at this angle the counter response is discriminatory with index of refraction for a given size, and the signal is strong enough. A larger angle decreases the signal, and a smaller angle decreases the separation of the index of refraction-dependent counter response curves.

[20] By measuring scattering at two angles, two unknown particle properties, for example size and real index of refraction, can be determined if the particles are assumed to be spherical and nonabsorbing (imaginary index of refraction = 0). This can be achieved by using counter response ratio (CR_{40}/CR_{74}) and sum ($CR_{40} + CR_{74}$) [*Baumgardner et al.*, 1996]. In general, coordinate pairs of values of these parameters uniquely define particle size and refractive

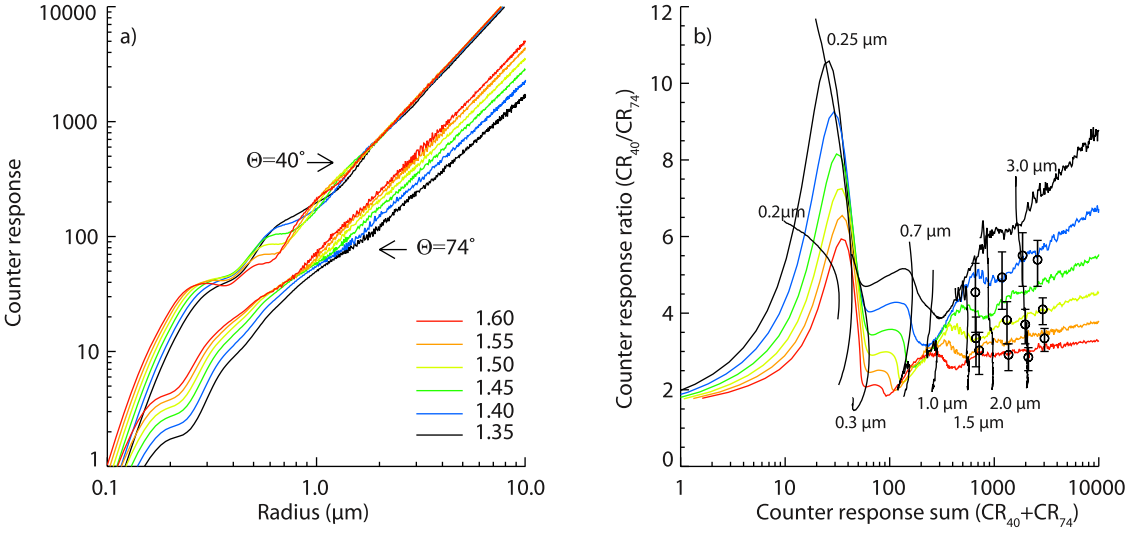

Figure 2. (a) Counter response (arbitrary units) at 40° and at 74° as a function of size for particles with indices of refraction ranging from 1.35 to 1.60. (b) Counter response ratio and sum (running average) for the same indices of refraction. Thin vertical lines are counter response ratio and sum for particles of 0.2, 0.25, 0.3, 0.7, 1.0, 1.5, 2.0, and 3.0 μm in radius. Also shown is the standard deviation for four sizes (1.7, 2.4, 3.0, and 3.62 μm) for indices of refraction of 1.40, 1.50, and 1.60. The standard deviation is determined from measurements described in section 3.2.

Table 1. Viscosity, Surface Tension, and Correction Factor of the Oils Used by *Baron et al.* [2004] (Denoted as b in Source Column) Which Gave Reasonable Fit[a]

Oil/index of Refraction	Density (g/cm^3)	Viscosity (Pa s)	Surface Tension (N/m)	Δ_a/a_p^2	Source
Oleic acid	n/a	0.026	0.032	0.024	b
Polydimethylsiloxanes 200/50	n/a	0.05	0.021	0.020	b
Polydimethylsiloxanes 200/50	n/a	0.10	0.021	0.021	b
Polydimethylsiloxanes 200/50	n/a	0.20	0.021	0.007	b
Polydimethylsiloxanes 200/50	n/a	0.50	0.021	0.004	b
DEHS 1.455	0.91	0.023	0.032	0.026	t
Cargille series A 1.51	0.91	0.032	0.031	0.021	c
Cargille series AA 1.40	0.93	0.009	0.019	0.066	c

[a]The oils used in this research are the 3 last in the table. Density is also shown for these oils. Sources: b: *Baron et al.* [2004], t: *TSI* [2006], and c: Cargille Labs.

index, as shown in Figure 2b. For particles >1.9 μm, the size can first be determined, using measurements at 40°, where counter response is insensitive to index of refraction. Index of refraction is then determined using measurements at 74°, or the counter response ratio. This index of refraction can subsequently be used to re-estimate the size by modifying the counter response function with the new index of refraction value. This process is repeated iteratively to convergence. A simpler and more accurate method involves the combination of counter response ratio and sum for particles with radius >1.9 μm since there is some variation in counter response at 40° for particles with different indices of refraction. For example, for a 2.5 μm particle, the difference in counter response for indices of refraction of 1.31 and 1.59 is about 6%, which results in a size difference of about 4%.

[21] Index of refraction cannot be determined for all sizes or indices of refraction. There are regions where the counter response sum and ratio overlap (Figure 2b). For example, for indices of refraction between 1.5 and 1.6 and particle size between 0.7 and 1 μm (a few selected sizes are shown as thin vertical lines in Figure 2b), the counter response at 74° cannot be differentiated. For particles between 0.25 and 0.3 μm, the counter response sum is not significantly different for all indices of refraction, so that refractive index and size cannot be determined in this region. Consequently, TAOPC applications are restricted to particles of radius 0.9 to 6 μm that have negligible absorption in this work.

[22] While the index of refraction of particles is frequently wavelength-dependent, the true index of refraction determined with the TAOPC is an integration over white light. Since the *QE* of the PMT and intensity of the light source in the TAOPC are both functions of wavelength, the index of refraction that is estimated with the TAOPC is assumed to be the weighted average index of refraction from 0.3 to 0.7 μm, the wavelength range where the PMTs are sensitive:

$$m_{ave} = \frac{\sum_{0.3\,\mu\mathrm{m}}^{0.7\,\mu\mathrm{m}} m(\lambda) I_0(\lambda) QE(\lambda)}{\sum_{0.3\,\mu\mathrm{m}}^{0.7\,\mu\mathrm{m}} I_0(\lambda) QE(\lambda)}. \quad (2)$$

3. Index of Refraction Determination of Spherical Nonabsorbing Particles

[23] The TAOPC was tested in the laboratory using four different particle types with different real indices of refraction. The particles used were spherical polystyrene latex (PSL) beads, and 3 oils with different compositions and indices of refraction: bis (2-ethylhexyl) sebacate (DEHS) and 2 oils from Cargille Labs (Series A 1.51 and AA 1.40) index of refraction liquid. Monodisperse oil particles were created with a Vibrating Orifice Aerosol Generator (VOAG 3450, TSI, Inc. St. Paul, MN). The size limitation for this instrument is 0.5 to 100 μm in radius. The average geometric standard deviation is 1.014 [*Berglund and Liu*, 1973]. An Aerodynamic Particle Sizer (APS) was used to determine particle size for comparison with the TAOPC. The APS measures aerodynamic particle size, a_a, where $a_a = \sqrt{\rho}\, a_p$ for solid spherical particles of radius a_p and density ρ [e.g., *Willeke and Baron*, 1993]. For liquid particles, droplet deformation must be accounted for in the APS. As the oil droplets in the air sample accelerate they deform into oblate spheroids due to drag in the strong acceleration field. The droplets flatten perpendicular to the airflow and thus the drag in the direction of the airflow increases. The increased drag leads to increased velocity of the oil droplets. Consequently the size of the droplet is underestimated [*Baron and Willeke*, 2001]. *Baron et al.* [2004] studied this deformation and how the size determination changed with particle size and composition by comparing size determined with the APS and aerodynamic size determined from settling velocity. They developed an empirical equation to correct for the deformation as a function of the surface tension, σ_l, and viscosity, υ_l, of the liquid. The size shift (in radius), Δ_a, can be found from the correction factor

$$\frac{\Delta_a}{a_p^2} = \frac{2\mathrm{a}}{\sigma_l^{\mathrm{b}} \upsilon_l^{\mathrm{c}}}, \quad (3)$$

where a = $1.222 \cdot 10^{-4}$, b = 0.5956 and c = 0.6916. This equation was fit to measurements on liquids which had a surface tension in the range of 0.031 to 0.0489 Nm^{-1} and viscosity in the range of 0.025 to 0.6 Pa s [*Baron et al.*, 2004] (see Table 1). The estimated geometric radius of the liquid particle a_g is then

$$a_g = a_p + \Delta_a. \quad (4)$$

3.1. Particle Radius and Index of Refraction Determination

[24] The TAOPC was calibrated with 2 μm PSL particles. Because PSL particles have a wavelength-dependent index of refraction, the TAOPC is sensitive to the weighted

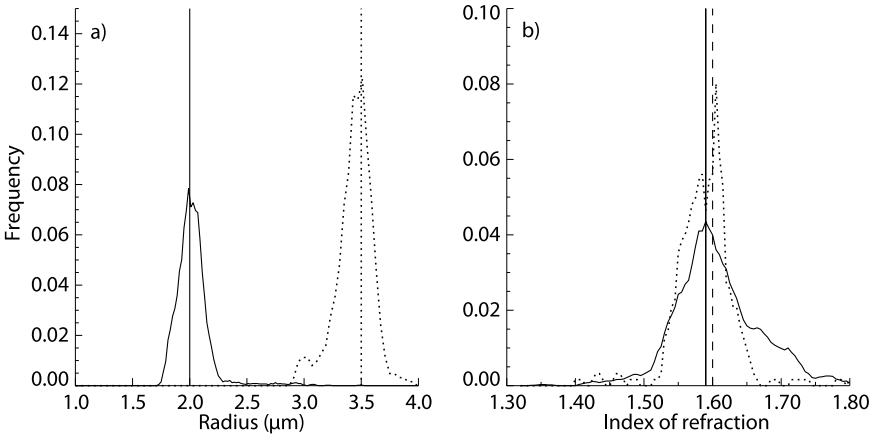

Figure 3. Estimated radius (a) and index of refraction (b) for 2 μm (solid line) and 3.5 μm (dotted line) PSL particles. Vertical solid and dotted lines are the expected values, and the dashed line in Figure 3b shows the estimated index of refraction for both sizes.

average PSL refractive index (equation (2)). *Ma et al.* [2003] determined a wavelength-dependent PSL index of refraction used here to calculate the weighted average PSL index of refraction for the TAOPC (1.591).

[25] Size and index of refraction determination for these calibration particles serves as the first test of the size and index of refraction technique used here. Figure 3a shows the estimated size (solid line) of a sample with 2 and 3.5 μm PSL particles. The median estimated sizes for these samples are 1.99 and 3.42 μm. Figure 3b shows the estimated indices of refraction for PSL where the median estimated index of refraction is 1.60. The distributions of the estimated indices of refraction are not normally distributed even though the counter response ratio distribution is close to normal (not shown). This is because of the convergence of counter response ratio curves for increasing indices of refraction (see Figure 2b). The index of refraction distribution at 3.5 μm is narrower than for the 2 μm PSL particles, which is expected since measurement uncertainties are less at increasing sizes. The non-normal index of refraction distribution is most noticeable for high indices of refraction where the different counter response ratio curves are closer, than for low indices of refraction. The estimated indices of refraction from these two samples are both 1.60, close to the expected value of 1.591, showing that the method used to determine particle size and index of refraction of pure scattering particles is robust.

[26] The liquid oil particles (DEHS, and Cargille Series A 1.51 and AA 1.40 index of refraction liquids) were generated with the VOAG at several different sizes. A total of 53 monodisperse particle distributions with sizes ranging from about 1.9 to 5.1 μm were generated with the different types of oil. The sizes determined with the TAOPC are compared with the uncorrected APS measurements in Figure 4a, while Figure 4b shows the APS sizes corrected for deformation, using the empirical equation 4 and the surface tension and viscosity values given in Table 1. The percent differences between the sizes determined with the two instruments are shown in Figure 4c for the uncorrected and Figure 4d for the corrected size. For each different oil, a linear regression is fit to the size difference (solid lines with the respective symbols plotted on the lines). Also shown in Figure 4c and 4d are measurements from *Baron et al.* [2004] for oleic acid (dashed line). The calculated deformations of the 3 different oils used here show the same tendency and have close to the same values (Figure 4c); they are all comparable with the results from *Baron et al.* [2004].

[27] The surface tension and viscosity of oleic acid are comparable with DEHS and 1.51 Cargille series A (see Table 1). The APS sizes for DEHS and 1.51 Cargille series A both approach the sizes determined with the TAOPC after applying the APS deformation correction. In contrast, most 1.40 Cargille series AA particle sizes from the APS, after deformation correction, are larger than the TAOPC estimates. From the measurements, the difference in distortion between the 3 oils are not large, while the correction factor for the 1.40 Cargille series AA oil is about three times that of the DEHS and 1.51 Cargille series A oils (Table 1). The large correction factor of the 1.40 Cargille series AA oil is because of the fact that the 1.40 Cargille series AA has a lower viscosity and somewhat lower surface tension compared to the 2 other liquids used here. Some liquids in Table 1, used by *Baron et al.* [2004] for developing equation (4), have similar surface tension values as 1.40 Cargille series AA oil. However, their viscosities are much greater than that of the 1.40 Cargille series AA oil. Therefore equation (4) is probably not completely appropriate for particles with such low viscosity.

[28] The close agreement between the measured APS size and measurements by *Baron et al.* [2004] before correction, when compared with TAOPC size (Figure 4c), suggests that the TAOPC size determination is acceptable. Furthermore, the sizing errors of PSL particles by the TAOPC were small, being only 0.5 and 2.3% for the 2.0 and 3.5 μm particles, respectively.

[29] Simultaneously with the size determination of the 3 different types of oils, indices of refraction were determined for the 53 monodisperse particle distributions. For a comparison between estimated and reference values, the weighted average index of refraction of DEHS particles over white light, as determined with the TAOPC is calculated from equation (2), and yields a value of 1.455. The wavelength-dependent refractive indices were found in *TSI* [2006]. For the 1.51 and 1.40 Cargille oils, the weighted indices of

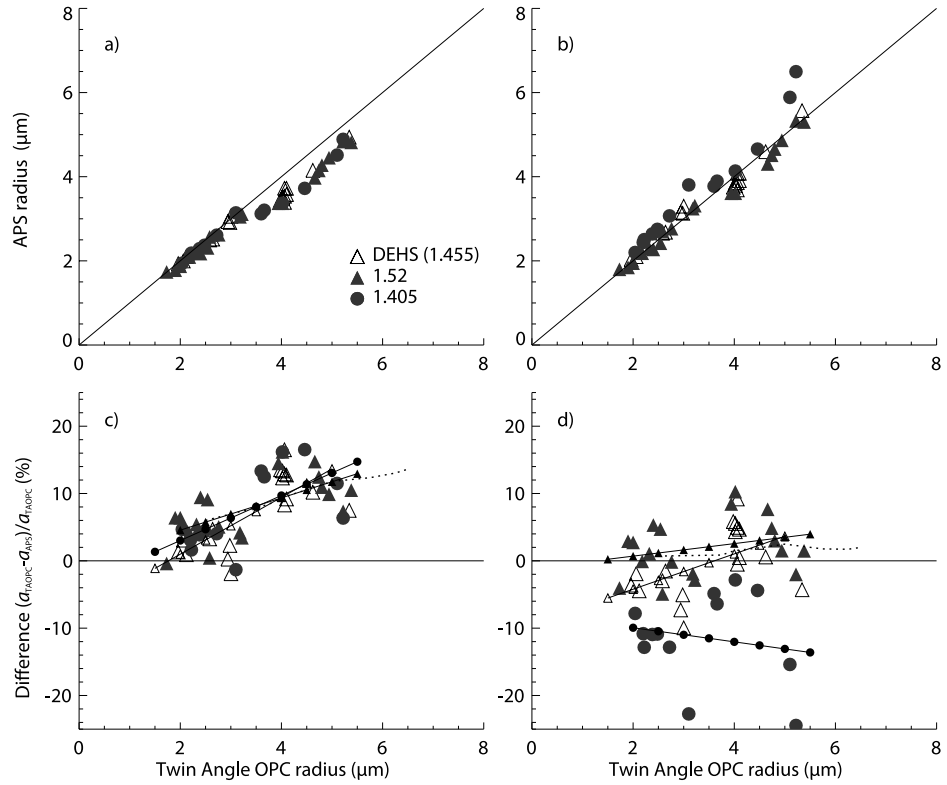

Figure 4. (a) Sizes determined with the TAOPC and uncorrected APS sizes. Solid line is the one-to-one relationship. (b) Same as in Figure 4a but for corrected APS sizes. (c) Percent difference between TAOPC and uncorrected APS sizes. Dashed line indicates measurements by *Baron et al.* [2004] with oleic acid, where aerodynamic size determined with the APS was compared to aerodynamic size determined by settling velocity. Solid lines (with small symbols) are linear regressions for the respective oils. (d) Same as in Figure 4c but for the corrected APS sizes.

refraction reported by the manufacturer are 1.52 and 1.405 respectively.

[30] Figure 5a shows the estimated indices of refraction for 55 monodisperse particle distributions as a function of estimated size, including the 2 and 3.5 μm PSL particles. The average indices of refraction determined for all distributions of the same type of particle, compared to, in parenthesis, the weighted average indices of refraction from the literature are: PSL: 1.60 (1.591); DEHS: 1.454 (1.455); 1.51 Cargille series A: 1.515 (1.52); 1.40 Cargille series AA: 1.409 (1.405). The error bars in Figure 5a are one standard deviation of the index of refraction distributions

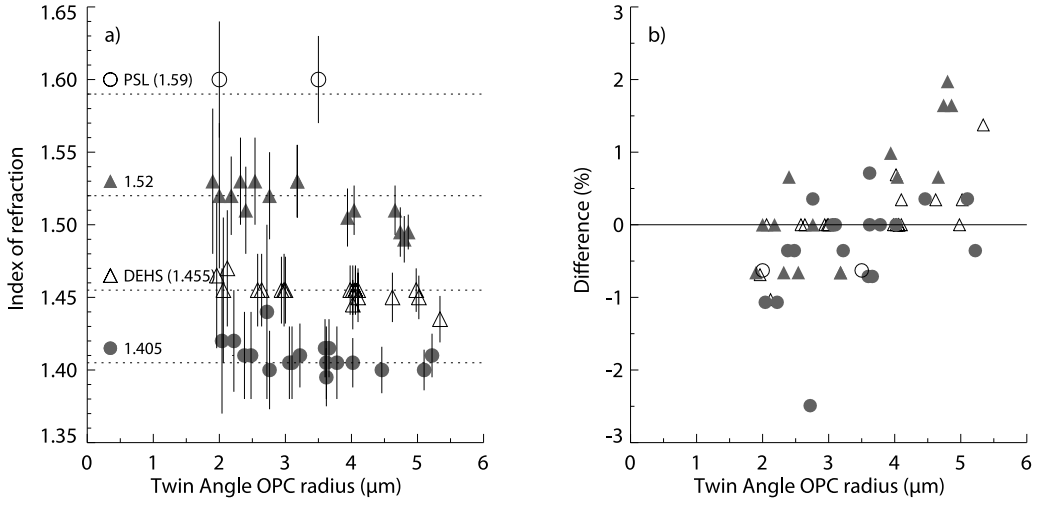

Figure 5. (a) Estimated indices of refraction for three oils and PSL particles. Error bars are one standard deviation. (b) Percent difference of the estimated indices of refraction.

which can be described with Gaussian distributions, except for those for PSL. Because the counter response ratio curves converge for high indices of refraction (Figure 2b), the distributions for PSL particles deviate from a Gaussian distribution (Figure 3b, solid line); however, for 2 and 3.5 μm particles, the distributions were close enough to Gaussian to estimate a standard deviation. Figure 5b shows the percent difference between the estimated and weighted average index of refraction. Most of the estimated indices of refraction are within ±1% of the weighted average index of refraction.

3.2. Estimated Measurement Uncertainties From Studies of Spherical Nonabsorbing Particles

[31] Measurement uncertainties can be determined from the observations of the monodisperse PSL and the oil particles described above. The main uncertainties are photoelectric statistical broadening in the PMTs, and to a smaller extent non-uniform illumination (section 2.1). *Miao* [2001] evaluated the effect of statistical broadening by the PMTs. Uniform square wave pulses were generated and fed into a light emitting diode lamp which was fixed to the sensitive areas of the PMTs directly, thus non-uniform illumination and coincidence are not issues. The results from the investigation by *Miao* [2001] are compared with the measurement uncertainties described here to determine the effect of non-uniform illumination and other observational uncertainties.

[32] The measured counter response distributions are near normal and can be expressed as a Gaussian distribution with standard deviation (σ) and mean (μ). Standard deviations of counter response at 40° and 74° are shown in Figures 6a and 6c for 55 measured size distributions with monodisperse aerosols. The coefficients of variability ($CV = 100\% \cdot \sigma/\mu$, i.e., relative uncertainties) are shown in Figures 6b and 6d for 40° and 74° respectively. Fitted power regressions of measured standard deviation as a function of counter response are shown as solid lines. The relatively slow increase in standard deviation compared to the increase in counter response is another indication of the effect of PMT pulse width broadening. The slow increase in standard deviation indicates that the broadening is relatively constant and independent of signal strength, thus *CV*, or the relative uncertainty, decreases as size increases.

[33] Measurement uncertainties determined here are compared to those due to photoelectric statistical broadening in the PMT at 40°, determined by *Miao* [2001]. The PMT uncertainties are shown as dotted lines in Figure 6a and 6b. They are given as a linear regression of the full width at half maximum (FWHM) as a function of counter response. For Figure 6 it was assumed that the measurements in the study of *Miao* [2001] were normally distributed and the standard deviations were calculated on the basis of a normal distribution with the same FWHM. The dashed line shows a linear regression of the standard deviation of the 55 distributions measured here. The uncertainties now determined compare well with those determined by *Miao* [2001] and indicate again that photoelectric statistical broadening by the PMT is the main source of measurement uncertainty. This was also observed by *Pinnick and Hofmann* [1973]. Comparison at 74° with results from the study of *Miao* [2001] could not be performed because the calibrations used different gain stages.

[34] Figure 7 shows, as a function of particle size, the relative uncertainties of the index of refraction distributions, CV_{index} (left axis). The CV_{index} is created following the analysis of counter response ratio and sum. CV_{index} decreases as particle size increases, which is in agreement with the decrease in CV of CR_{40} and CR_{74} with increasing size (Figure 6). The regression of the relative uncertainties (shown as solid curve) for index of refraction as a function of particle size, for particles between 2 and 6 μm, is given as:

$$CV_{index} = 5.98 a_p^{-1.12}. \quad (5)$$

Equation (5) is valid for the indices of refraction used in this study which are between 1.40 and 1.60. Figure 7 shows that the relative uncertainties for a given size do not change with index of refraction and equation (5) can be used to estimate uncertainties in the determination of index of refraction based only upon particle size. The related counter response ratio standard deviation, on the other hand, has a larger variation as a function of index of refraction (Figure 2b). This is because of the larger range of counter response ratio values, and that the relative difference between counter response ratios is larger than the relative difference of the respective indices of refraction.

[35] The measured index of refraction distributions are relatively narrow (CV_{index} between 1 and 4%), a necessary attribute for determining an exact particle index of refraction and to differentiate between particles with different indices of refraction when the range of indices of refraction is small. The index of refraction, size and measurement uncertainties determined here are for spherical nonabsorbing particles.

[36] We note that uncertainties less than 4% might still be large since index of refraction of atmospheric aerosols tends to range only between 1.3 and 1.7. To illustrate the width of the index of refraction distributions in absolute values in Figure 7 we show examples of the absolute uncertainties (standard deviation) in indices of refraction determination as a function of CV_{index} for three different values of index of refraction (diamond symbols in red, with axis at the top).

[37] The TAOPC was also tested with high gain settings for the PMTs to allow for measurements of particles less than 0.9 μm; however, high gain settings resulted in large relative uncertainties. For 0.5 μm PSL particles, CV_{40} was 25% and CV_{74} was about 30%, leading to a counter response ratio distribution which was too wide for an index of refraction determination to be achieved with low uncertainty.

4. Index of Refraction Determination of Non-Spherical Absorbing Particles

[38] The TAOPC was, in addition to tests in the lab, also tested with a sample of ambient aerosols. The measurements were conducted in a small urban mid-continental North American location (Laramie, Wyoming). The instrument was configured such that it was sensitive only to particles

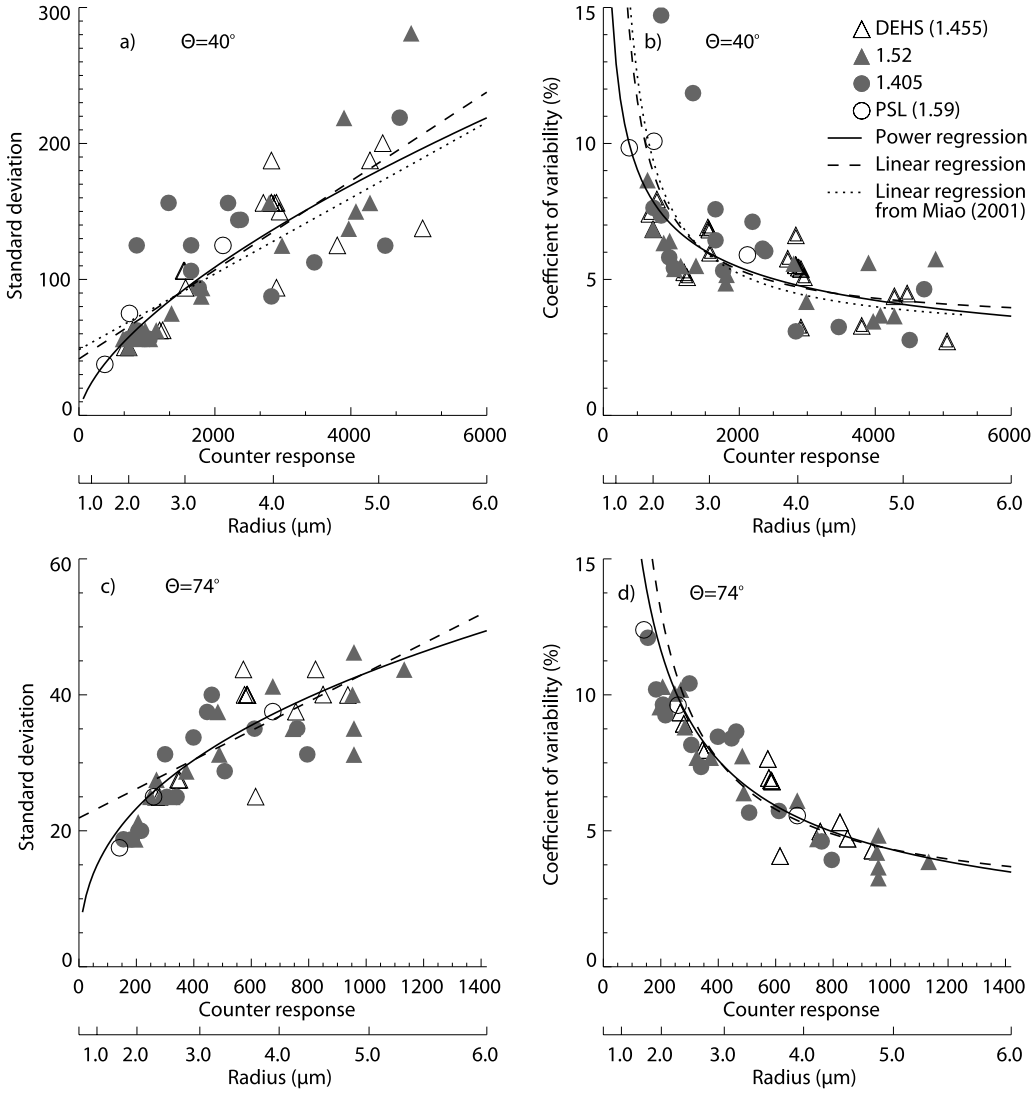

Figure 6. (a and c) Standard deviation (arbitrary units) for all 55 monodisperse aerosol samples (including 3 PSL samples) as a function of counter response (arbitrary units) at 40° and 74°, respectively. Solid lines are power regressions. For comparison, linear regression at 40° of the standard deviation measured here (dashed line) and PMT measurement uncertainties found by *Miao* [2001] (dotted line) are shown. The size scale at the bottom is somewhat approximate, as size is not a linear function of counter response. Here an index of refraction of 1.50 is assumed for the conversion from counter response to size. (b and d) The relative uncertainties/coefficient of variability (*CV*) for the 40° and 74°, respectively.

greater than ~0.9 μm. Thus the observed ambient aerosols contained primarily dust particles.

[39] For the measurements of dust particles with the TAOPC, outside air was brought into the aerosol laboratory through a 7.3 cm diameter ambient air intake. The temperature in the air intake was controlled so the relative humidity did not exceed 25%. The intake was located on the roof of a building approximately 20 m above the ground. Simultaneously with the TAOPC measurements, a filter pack system containing a 47 mm diameter polycarbonate filter with 1 μm pore size collected particles for analysis of their composition. The flow rate through the filter was 5 LPM. This filter was analyzed using the Computer-Controlled Scanning Electron Microscopy (CCSEM) technique by the RJ-Lee group (R. J. Lee Instruments, Ltd., Trafford, PA). The CCSEM technique allows for an automated analysis of particle size and elemental composition where size and composition are found by combining a scanning electron microscope (SEM), X-ray analyzer and digital scan generator under computer control.

[40] The TAOPC and polycarbonate filter measurements were carried out on February 22, 2006, for about 2 hours. These measurements were conducted as part of a more extensive investigation of tropospheric aerosols, designed to study the dependence of aerosol radiative and hygroscopic properties on particle chemical and physical properties. A variety of aerosol instruments were used for this effort. Of interest here are size distributions for particles >0.5 μm with the APS and two additional sets of filter pack systems. One set collected total suspended particulate (TSP), while the other, installed downstream of a cyclone separator, collected particulate matter smaller than 0.5 μm ($PM_{0.5}$) in radius.

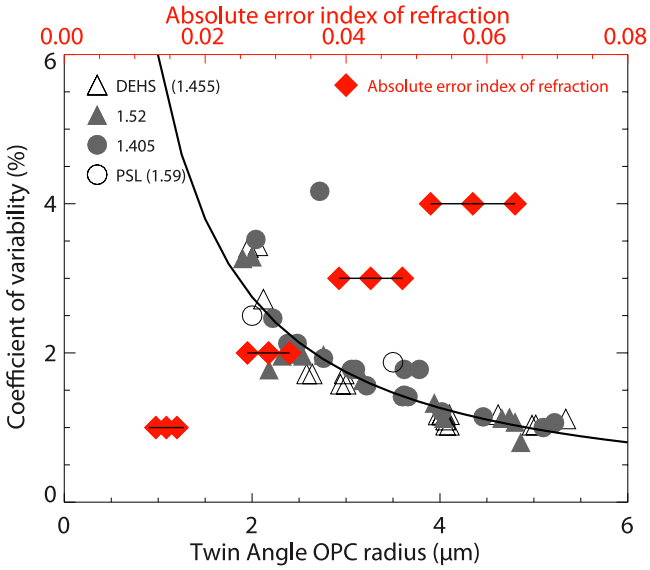

Figure 7. Coefficient of variability of index of refraction for all samples as a function of size, left and bottom axis. Solid line is regression of the CV_{index}. Also shown, in red diamonds with axis at the top, are the absolute errors (one standard deviation) in index of refraction as a function of CV_{index}. The errors are calculated from $CV_{index}/100 \cdot n$ where n = 1.3, 1.45, 1.6 corresponding to the left, middle, and right red diamond for each CV_{index} group.

Each set of filter systems had two filter pack channels (Channel I and Channel II). Channel I had a Gelman PTFE Teflon-membrane filter backed by a Pallflex Quartz filter and Channel II had a Pallflex Quartz filter backed by a sodium chloride impregnated Whatman 41 cellulose fiber filter. All filters were 47 mm in diameter. Sample collection times ranged from 24 to 48 hours and flow rate was ~21 LPM. The filters were prepared and analyzed by the Energy and Environmental Engineering Center at the Desert Research Institute (DRI) in Reno, Nevada. The total aerosol mass loading was determined with gravimetric analysis of the Teflon filter and non-dispersive X-ray fluorescence spectrometry was used for elemental mass loadings. Other analytical techniques were also used to determine quantity and presence of elemental species, however these species were mostly small sized non-mineral material. Since the lower size limit of the TAOPC is about 0.9 μm in radius, comparisons between filter and TAOPC measurements used the particulate compositions derived by taking the difference between the observed TSP and $PM_{0.5}$ species mass loadings, found to result primarily from mineral material.

4.1. Index of Refraction Determination From TAOPC Measurements Using Particle Number Ratio Approach

[41] It is anticipated that some of the dust particles absorb, therefore a third unknown (imaginary index of refraction) is introduced to the TAOPC measurements in addition to size and real index of refraction. In this case the use or counter response ratio and sum cannot be used for index of refraction determination since there are several different solutions for complex indices of refraction that fit the measured scattering at 40° and 74°. In addition, most dust particles are non-spherical; however, for simplicity, we assume here that the measured particles are spherical. With this assumption another technique, particle number ratio, is used to determine complex index of refraction.

[42] The particle number ratio (PNR) approach [*Hu et al.*, 2006] to determine size distribution and complex index of refraction of particles within an ambient air sample, where scattering is measured at two angles, requires little post data processing. *Hu et al.* [2006] used a dual angle OPC, measuring scattering at 60° and 90°, as compared to the TAOPC's 40° and 74°. Following *Hu et al.* [2006], the estimated size distributions at the two scattering angles are only equal when the correct complex index of refraction is assumed. To determine the measured size distributions and complex index of refraction from the TAOPC, the number of particles in four different size regions at 40° ($N_{40}(a_{ai}, a_{zi})$) and 74° ($N_{74}(a_{ai}, a_{zi})$) are compared for several different complex indices of refraction, where a_{ai} and a_{zi} are the first and last size in size bin i = 1, 2, 3 and 4. Only for the correct real (n) and imaginary (k) index of refraction, will the PNR in all four size bins intersect and have a value near unity:

$$PNR_i = \frac{N_{40}(a_{ai}, a_{zi})}{N_{74}(a_{ai}, a_{zi})}. \tag{6}$$

Here PNR_i is calculated for each n from 1.45 to 1.7 in steps of 0.01 and for each k from 0.0 to 0.03 in steps of 0.001 and from 0.032 to 0.1 in steps of 0.002. For each n, the four PNR are compared over all k values. The estimated complex index of refraction is determined to be where the four PNR intersect close to unity. The intersection point will, for a real aerosol sample, have a small deviation from unity due to small errors in the calculation of the two size distributions [*Hu et al.*, 2006]. The inversion procedure therefore searches for the complex index of refraction that gives an average $\overline{PNR} = \sum_i PNR_i/4 \approx 1$. Several complex indices of refraction may fulfill this requirement, but many are associated with poorly characterized coincident PNR_i intersection points, even though the average PNR = 1. Therefore the inversion procedure also requires that all PNR_i must have a minimal deviation from $\overline{PNR}$. *Hu et al.* [2006] required that the deviation must be less than 5% for each individual PNR_i. Here we search for the complex index of refraction that gives the smallest deviation, d, from;

$$d = \min\left(abs\left(\sum_i \frac{\overline{PNR} - PNR_i}{\overline{PNR}} \right) \right)_m. \tag{7}$$

The simplicity of this technique is that only the voltage measured corresponding to a_{ai} and a_{zi}, based on the theoretical counter response and calibration of the TAOPC, needs to be determined. All values between a_{ai} and a_{zi} can be taken directly from the raw voltage data. Thus $N_{40}(a_{ai}, a_{zi})$ and $N_{74}(a_{ai}, a_{zi})$ are given by all measured voltages between the two precalculated theoretical limits for size bin i. This method can give an average complex index of refraction for a sample containing many particles, but cannot give an index of refraction of each particle in the sample. However, because of non-spherical particles and multiple solutions for absorbing particles, it is generally

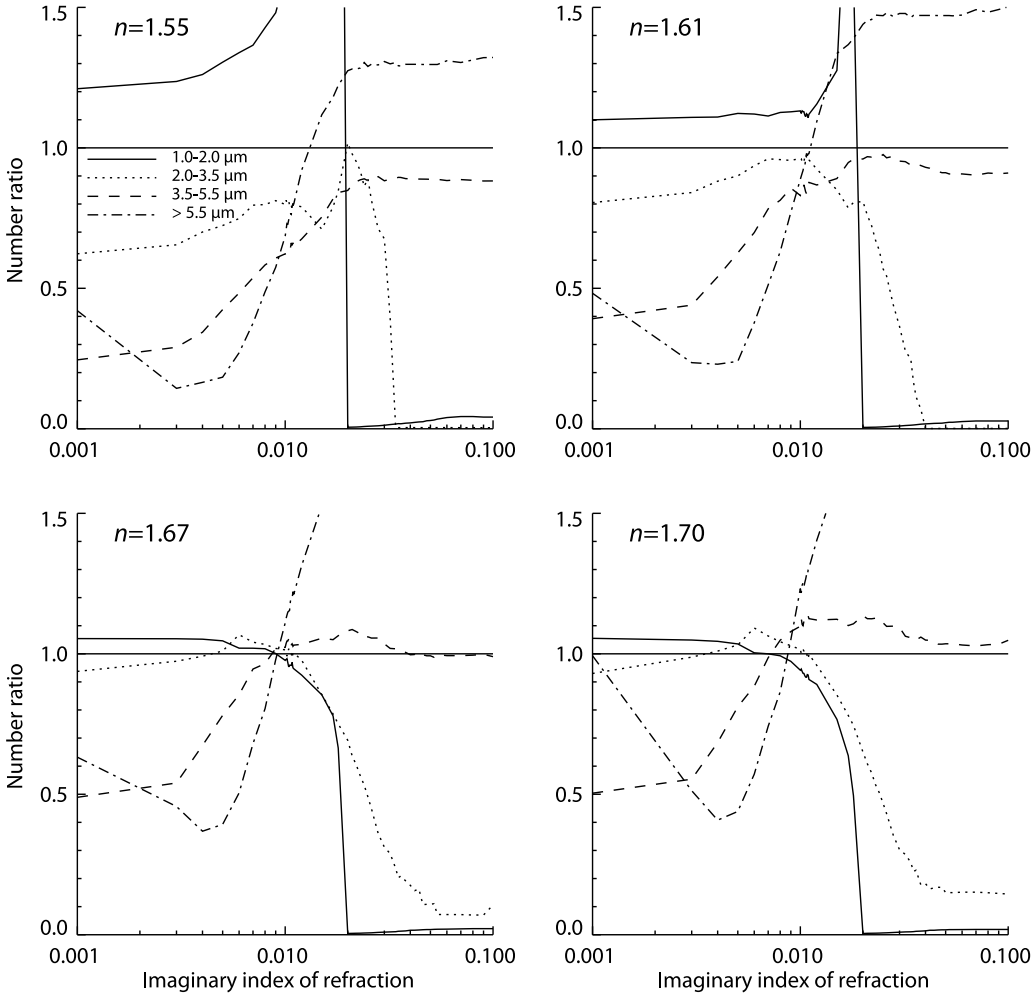

Figure 8. PNR as a function of imaginary index of refraction (k) for four size ranges (1.0–2.0, 2.0–3.5, 3.5–5.5, and >5.5 μm) for several different real indices of refraction (n) shown at the top of each panel.

difficult to determine the index of refraction of single particles for samples of this type.

[43] Within the two hour experimental period, scattering data were obtained for about 12,000 particles with radius >1 μm. Size bins were allowed to vary until the four calculated *PNR* values gave at least one acceptable intersection point, as described above. If the size bins are too small, no solutions are found. For this analysis, size bins were fixed at 1.0–2.0, 2.0–3.5, 3.5–5.5 and >5.5 μm. Figure 8 shows PNR_i from the TAOPC measurement as a function of k for several different n. The best fit is $m = 1.67 - 0.009i$, for which $\overline{PNR}$ is 1.018. The deviations from the average *PNR* for size bins 1, 2, 3, and 4 respectively are 0.74, −0.11, −0.08 and −0.54%, corresponding to a 1.48% deviation from $\overline{PNR}$ (from equation (8)). Some variations of estimated index of refraction were found with small variations in the size bins. These variations are in the range $1.64 - 0.0104i$ to $1.67 - 0.009i$.

4.2. Effect of Non-sphericity on Measurements

[44] Scanning electron microscope images show that mineral dust and soil particles are mostly non-spherical [e.g., *Reid et al.*, 2003; *Clarke et al.*, 2004; *Shi et al.*, 2005]. *Hill et al.* [1984] determined an average shape distribution of soil particles, with prolate particles having a peak aspect ratio of about 2.2 and oblate particles a peak aspect ratio around 0.5. Patterns from two-dimensional angular optical scattering measurements in Baltimore-Washington show that 45% of 505 particles of a nominal size of 1 μm were spheres or perturbed spheres, while for nominal sizes of 2.5 μm, only 5% were spheres or perturbed spheres [*Aptowicz et al.*, 2006]. *Pinnick and Rosen* [1979] measured non-spherical doublet polystyrene latex aerosols with Knollenberg light-scattering counters and noticed that the measured counter response distribution width increased for non-spherical particles, even though all the non-spherical particles were almost identical in size and shape. This broadening is due to the different orientations of the particles in the scattering volume.

[45] From the 2 hours of measurements in February, the measured counter response ratio distribution from the TAOPC can be constructed. This distribution can also be modeled, using size distributions from the APS that was measuring simultaneously with the TAOPC, to calculate a theoretical counter response ratio distribution. Figure 9 shows both the measured (solid line) and modeled (broken lines) counter response ratio distributions. The dashed curve shows the modeled counter response ratio using measure-

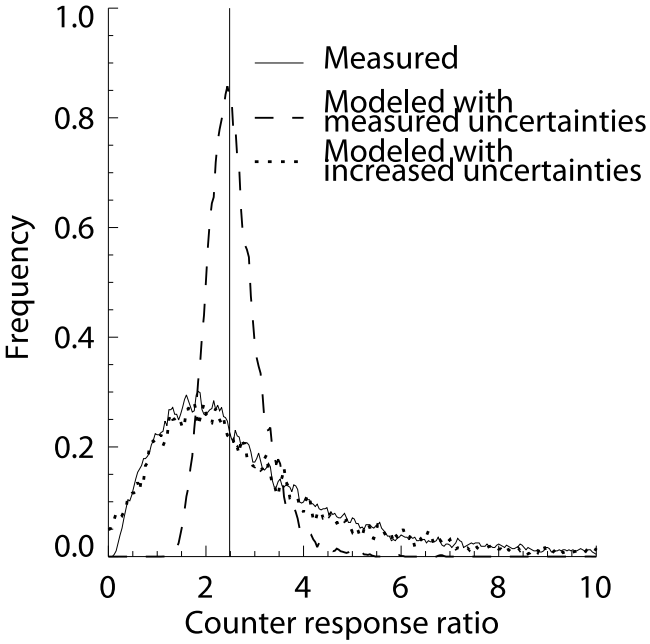

Figure 9. Measured counter response ratio distribution (solid curve). The dashed curve shows modeled counter response ratio distribution assuming $m = 1.67-0.009i$ and using measured APS size distribution and TAOPC measurement uncertainties determined with spherical particles in the laboratory. The dotted curve shows the modeled counter response assuming increased measurement uncertainties with a factor of 4.5 at 40° and 3.5 at 74°.

ment uncertainties determined with spherical particles in the laboratory (section 3.2), and assuming the measured index of refraction of $1.67-0.009i$. Both the solid and dot dashed curves have the same median (solid vertical line), which corresponds to particles with the average estimated index of refraction; however, the modeled counter response ratio is much narrower than the measured counter response ratio. The dotted curve shows a modeled counter response ratio when measurement uncertainties are increased (4.5 times at 40° and 3.5 times at 74°). This compares well with the measurements, suggesting the ambient particles measurements have a larger uncertainty than indicated by the laboratory measurements. A population of non-spherical particles would increase measurement uncertainties due to random orientation of the particles and variations in scattering from non-spherical particles. In addition to shape, but to a smaller extent, a polydisperse index of refraction distribution will also increase the counter response ratio distribution. The increase in the distribution width does not give information about the shape of the particles, only an indication of the effects of the sampling of non-spherical particles and a polydisperse index of refraction distribution on TAOPC measurements.

[46] Mie scattering theory is used here for the TAOPC index of refraction determination, while the broad counter response ratio distribution indicates that the particles measured are non-spherical (in agreement with *Hill et al.* [1984], *Reid et al.* [2003], *Clarke et al.* [2004], and *Aptowicz et al.* [2006]). *Mishchenko et al.* [1997] show, with the use of the transformation matrix (T-matrix), that the difference in phase function between spherical particles and spheroids can be large, especially for side (>90°) and backscatter where the differences can be several hundred percent. The differences are generally less at forward directions (<90°) and are also less for prolate than oblate spheroids. They also show that if particles in a sample have a large distribution of different shapes, the difference in the phase function between non-spherical and spherical particles decreases. In addition, the difference in the phase function decreases with increasing imaginary index of refraction. The difference in scattering cross section (integration of the phase function over all solid angles) between non-spherical particles in a broad shape distribution and spherical particles is much smaller than the phase function at specific angles. Uncertainties in the index of refraction determination are therefore mainly introduced in the phase function at the measured angles by assuming that the measured particles are spherical in shape instead of accounting for real shape. These uncertainties are decreased if the particles in the sample measured have a broad range of shapes and sizes.

[47] An error analysis of the PNR approach for determining index of refraction was based on published T-matrix calculations and optical measurements of ensembles with particles having broad shape and size distributions. The use of broad shape and size distribution are due to two factors. First, the TAOPC has a white light source (wavelength ranging from 0.3 to 0.7 μm), thus each individual measured particle with a specific size has size parameters ranging from $2\pi \cdot a/0.7\mu$m to $2\pi \cdot a/0.3\mu$m, where a is the volumetric radius (typically 1 to 5 mm). Our measurements can therefore be compared with monochromatic optical measurements of particles with a distribution of sizes. Second, through the PNR approach, measured scattering from individual particles are combined to form ensembles over known size ranges. In these ensembles, there is a broad distribution of shapes.

[48] The error analysis was completed assuming errors in counter response according to Figures 1 and 2 and Plate 4 in the study by *Mishchenko et al.* [1997]. Plate 4 shows the ratio, δ, in calculated phase function between broad spheroid shape distributions and that of surface-equivalent spheres as a function of effective size parameter and scattering angle. For all angles that contribute to TAOPC scattered light detected by the PMT centered at 40° (angles from 23.4° to 56.6°), δ ranges from 1.0 to about 0.7, with a mean ratio, δ_{40}, in the range of 0.8–0.9, depending on the size parameter. For angles centered at 74° (angles from 55.2° to 92.8°), δ ranges from 0.7 (for the lower angles) to 1.3 (for the larger angles). The mean ratio, δ_{74}, is about 0.9–1.0. Overall δ_{40} may be lower than δ_{74} by approximately 5–10% for particles with an index of refraction of $1.53-0.008i$ as used by *Mishchenko et al.* [1997]. These differences in δ_{74} and δ_{40} are probably at the high end of what may be expected. Figure 1 of *Mishchenko et al.* [1997] indicates the ratio between theoretical phase functions for spheroids and spheres is $\delta_{40} \approx 0.9$ and $\delta_{74} \approx 0.95$ at 0.44 μm. Figure 2 from *Mishchenko et al.* [1997] shows measured phase function of soil dust from *Jaggard et al.* [1981] and calculated phase function for spheres and spheroids. The average ratio between the measured phase function

(from *Jaggard et al.* [1981]) and spheres (n = 1.53–0.0085i) is $\delta_{40} \approx 0.83$ and $\delta_{74} \approx 0.82$. Thus these two figures suggest the errors in phase function from non-spherical particles at the two angles are nearly the same. Slightly different errors may apply for other indices of refraction, but the differences are not expected to be large.

[49] The size parameters for the measurements by *Jaggard et al.* [1981] is from 12 to 31 (1 to 2.5 μm in radius for wavelengths of 0.5 μm). While the TAOPC size parameter range is about 9 to 100, for the wavelength with most contribution in the TAOPC ($\sim$0.5 μm) the size parameter ranges from 12 to 62. The TAOPC measurements therefore extend the measurements by *Jaggard et al.* [1981] but the size parameters in the study of *Jaggard et al.* [1981] are nevertheless a part of what is measured with the TAOPC.

[50] To estimate the impacts of non-sphericity on the PNR approach, the phase function ratios were used to represent the errors in counter response which would occur from assuming spherical particles for the inversion method instead of non-spherical particles. The following ranges of values for δ_{40} and $\delta_{74} - \delta_{40}$ were assumed: 0.8–1.1 and 0.0–0.2. For all cases when $\delta_{74} - \delta_{40} = 0$, there is no impact from non-sphericity on the estimated complex index of refraction. As $\delta_{74} - \delta_{40}$ increases the PNR approach estimates decreasing values of the real index of refraction, while the imaginary index of refraction is not affected. For $\delta_{74} - \delta_{40} = 0.1$ (0.2), the estimated real index of refraction decreases to 1.60 (1.55). These results are the same for all values of δ_{40}. As long as non-sphericity affects the phase function at the two angles similarly, $\delta_{74} - \delta_{40} = 0.0$, non-sphericity does not change the results of the PNR inversion. This result arises from the facts that $dCR_{40}/da \approx dCR_{74}/da$ over the size ranges considered here (see Figure 2a) and that the PNR approach deals with number ratio from 40° and 74° measurements and not individual number counts. When an error is assumed, the size range a_{ai} to a_{zi} in equation 6 changes. If the relative errors are the same at 40° and 74°, the new size range in ($N_{40}(a_{ai}, a_{zi})$) in equation 6 is close to the new size range for ($N_{74}(a_{ai}, a_{zi})$) (since $dCR_{40}/da \approx dCR_{74}/da$), and the index of refraction retrieved with the PNR approach is the same as assuming that the particles are spherical. The larger the difference of δ_{74} and δ_{40}, the more the estimated real index of refraction deviates from that assuming spherical particles or no differences in the magnitude of the phase function variations due to non-sphericity. This is because, in practice for the PNR approach, we are considering different size ranges for $N_{40}(a_{ai}, a_{zi})$ and $N_{74}(a_{ai}, a_{zi})$ when $\delta_{74} - \delta_{40} \neq 0$. The estimated imaginary index of refraction is not sensitive to non-sphericity based on this analysis.

[51] *Liu et al.* [2003] measured phase functions on quartz particles and compared them with Mie calculations. The measurements on quartz, however, are relative values of the phase function and thus must be normalized with a true phase function. *Liu et al.* [2003] attempt this by matching the Lorenz-Mie curves for spherical particles with the phase function measured on quartz in the extreme forward direction to create the "synthetic" phase function shown. According to these results, $\delta_{74} - \delta_{40}$ may be closer to 0.3, which leads to an estimated real index of refraction of about 1.51. However, *Liu et al.* [2003] are not convinced that their approach is entirely reliable and point out the errors and assumptions required to create the "synthetic" phase function. In particular, slight differences would reduce the value of $\delta_{74} - \delta_{40}$, bringing it more in line with the work of *Mishchenko et al.* [1997] and *Jaggard et al.* [1981]. In addition, quartz does not have an imaginary part. According to *Mishchenko et al.* [1997], the ratio δ tends to decrease with increasing imaginary refractive index. Overall, errors introduced into the PNR approach by non-spherical particles could indicate some overestimations of real indices of refraction.

[52] *Pinnick et al.* [1976] compared angular scattering measurements on monodisperse non-spherical sodium chloride and potassium sulfate particles with scattering by spheres of the same cross-sectional areas using monochromatic light. While these measurements show quite large differences at the angles of interest for the TAOPC (40° and 74°), there are problems in using them for our error analysis. The range of size parameter for measurements by *Pinnick et al.* [1976] (up to 8.4) is below the size parameter for the polychromatic TAOPC (9 to 100), and there is no clear way to extrapolate the *Pinnick et al.* [1976] measurements. The particles used by *Pinnick et al.* [1976] are non-absorbing and a single measurement represents results from a single size parameter. The TAOPC measurements are on absorbing particles and measurements on a single particle are the result of a distribution of size parameters due to the polychromatic light source. Both of these factors, absorption and polydisperse size parameter dampen the differences between non-spherical and spherical scattering [*Mishchenko et al.*, 1997]. For these reasons the results by *Pinnick et al.* [1976] could not be used in our error analysis.

4.3. Filter Data Results

[53] For the two hour polycarbonate filter samples, a CCSEM analysis was performed on particles on 17.37 mm^2 of the filter, corresponding to 1% of the total area. The analysis of this filter was divided into 3 size classes: 1.0–1.25, 1.25–2.5 and 2.5–10 μm, in which 69, 54 and 8 particles, respectively, were detected. For each size class, the fraction of the elements Na, Mg, Al, Si, P, S, Cl, K, Ca, Ti, Cr, Mn, Fe, Ni, Cu and Zn were found from the average relative X-ray counts attributed to each element. The amounts of P, Ti, Cr, Mn, Ni, Cu and Zn were negligible and are not included in further analysis. It is assumed that the elemental components are present as the specific chemical species listed in Table 2.

[54] The CCSEM filter pack analysis is compared with filter pack analyses from the long duration filters exposed during the February 2006 measurements from a continuous 48 hour collection period, on February 21–23 (mst) and as an 11 day average (February 16–26). The mass concentration for the February 21–23 period was 5.54 μg/m^3, while that for the 11 day average was 5.77 μg/m^3. Table 2 shows the average mass loading percentage for each non-negligibly small inorganic chemical species for the three size classes from the CCSEM analysis and from the long duration filter measurements. The relative mass loading of each chemical species from the CCSEM analysis is similar over the three size classes, except for a noticeable decrease in CaO with increasing size. The largest size class (2.5–10 μm) also differs slightly, with more salt in the

Table 2. Mass Percentage of Chemical Species (Column 2) Collected in 22 February for Three Size Ranges (CCSEM Analysis) and for the Long Duration Filter, 21–23 February, and Average 16–26 February Measurements, Columns 3–7[a]

Elemental Components	Compound	1.0–1.25 μm	1.25–2.5 μm	2.5–10 μm	21–23 February, 48-h Measurements	February Average	Density (g cm^{-3})	Molecular Weight (g mol^{-1})	PMR (cm^3 mol^{-1})	Index of Refraction
Cl, excess Na	NaCl	1.05	1.05	5.41	6.35	7.91	2.17	58.4	8.53	1.55
Excess Cl	NH_4Cl	1.92	2.87	7.39	0	0	1.53	53.4	12.6	1.64
N	$NaNO_3$	0	0	0	2.17	3.62	2.26	85.8	12.59	1.587
Mg	MgO	2.17	1.44	4.48	2.17	2.64	2.58	40.3	4.52	1.74
Al and Si	$KAlSi_2O_6$	11.8	15.6	20.2	12.4	11.0	2.47	218.	26.5	1.51
Excess Al	Al_2O_3	9.16	10.0	8.50	16.7	16.9	3.97	102.	10.6	1.76
Excess Si	SiO_2	41.0	39.8	47.9	40.6	33.7	2.64	60.1	7.43	1.55
Rich in Ca, S	$CaSO_4$	2.45	7.31	0	0	0	3.0	136.	15.4	1.49
Ca	CaO	26.2	19.1	4.16	12.8	18.5	3.32	56.1	7.48	1.84
Ti	TiO_2	0	0	0	0.42	0.43	4.23	79.9	9.18	2.58
Fe	Fe_2O_3	4.30	2.86	7.40	6.18	5.21	5.24	160.	22.2	3.01–0.68i

PMR, partial molar refraction.
[a] Physical constants used for complex index of refraction calculation [*Weast and Astle*, 1979–1980; *Stelson*, 1990], columns 8–10, and results of the index of refraction calculation, column 11.

form of NaCl and NH_4Cl. The relative mass loading from the 21–23 February measurements is similar to the CCSEM analysis, but with slightly more Al_2O_3. Not listed for the long-period filter measurements are possible organic material mass loading contributions, which may total 1.03 ± 1.02 μg/m^3. Quantitative assay of organics in larger particles is difficult and may be compromised in part by the inexact differentiation of mass assignment at the "cut-off" limit of the $PM_{0.5}$ cyclone used to size select the ambient particles for analysis. Thus some of the organic material ascribed to >$PM_{0.5}$ particles may actually be present in particles of radius smaller than 0.5 μm. Furthermore, mass loadings of accumulation mode organics, measured by aerosol mass spectrometry, during the period of TAOPC observations and CCSEM filter material collection, were particularly low (~0.4 μg/m^3). It therefore seems likely that particles in the size range detected by the TAOPC would contain negligible amounts of organic material. Analysis of several long duration (24–48 h) filter measurements made in July, 2005 (not reported here) show similar mass loadings for refractory materials, as do those of observations made in western Wyoming in 1996 [*Han*, 1999].

4.4. Index of Refraction Calculation From Filter Data

[55] The mean real index of refraction of a particle sample consisting of several different elemental components can be calculated using the partial molar refraction approach [*Stelson*, 1990]. All chemical constituents in the particle are assumed to be homogeneously distributed throughout the aerosol. The mean real index of refraction n is found from the molar refraction, R, of a condensed phase, where R is defined as

$$R = V\left(\frac{n^2-1}{n^2+2}\right) \tag{8}$$

Here V is the molar volume given in cm^3 mol^{-1}. Rearranging equation (9) gives an expression for the index of refraction:

$$n = \left(\frac{1+2^R/_V}{1-{}^R/_V}\right)^{1/2} \tag{9}$$

The fraction R/V is given by

$$\frac{R}{V} = \sum_i \frac{R_i}{M_i}[S_i], \tag{10}$$

where R_i is the partial molar refraction of the chemical constituent and M_i is the molar mass of the same component in g mol^{-1}. Here $[S_i]$ is the concentration of the chemical constituent i in g cm^{-3} where

$$[S_i] = X_i \sum_i \rho_i, \tag{11}$$

X_i is the fractional mass of the constituent in the aerosol, and ρ_i is the density of the molecular species in g cm^{-3}.

[56] The only strongly absorbing species suggested by the filter data are those that contain iron. Several oxides or other

Table 3. Calculated/Estimated Average Complex Index of Refraction From Filter Data and TAOPC

Size Range	Index of Refraction ($m = n - ki$)
1–1.25 μm (CCSEM)	$1.65-0.008i$
1.25–2.5 μm (CCSEM)	$1.627-0.008i$
2.5–10 μm (CCSEM)	$1.608-0.015i$
Long duration filters, 21–23 February 2006	$1.621-0.012i$
Long duration filters, average 16–26 February 2006	$1.653-0.01I$
Long duration filters, July 2005	$1.648-0.012i$
TAOPC	Real: 1.60–167 Imaginary: $0.009-0.0104i$

species may be present, of which hematite (Fe_2O_3), goethite (FeO(OH)) and magnetite (Fe_3O_4) are perhaps the most probable candidates [*Weber et al.*, 2000; *Arimoto et al.*, 2002; *Alfaro et al.*, 2004; *Lafon et al.*, 2006; *Shen et al.*, 2006]. In the absence of additional information, we presume that iron is present as hematite, the most ubiquitously found of these oxides [*Horvath*, 1995; *Claquin et al.*, 1999; *Sokolik and Toon*, 1999]. Another potential absorber is light absorbing carbonaceous material (LAC) which would be detected primarily as elemental carbon (EC) [*Malm et al.*, 1994; *Kirchstetter et al.*, 2004; *Andreae and Gelencser*, 2006; *Bond and Bergstrom*, 2006]. However, analyses of the available data of organic species mass loadings during the period of TAOPC measurements suggests that the $PM_{>0.5}$ EC mass loading was indistinguishable from zero, within experimental uncertainty. Consequently, we cannot determine with confidence the amount of LAC in the supermicrometer aerosol or assess its contribution, if any, to absorption. We therefore omit it when calculating the index of refraction. The imaginary index of refraction of particles containing a mass fraction X_i of absorbing material was calculated using the volume weighted refractive index (VWR) method [*Ouimette and Flagan*, 1982; *Hasan and Dzubay*, 1983]:

$$k = \frac{\overline{\rho}(k_i X_i)}{\rho_i}. \tag{12}$$

Here $\overline{\rho}$ is the mean density of the aerosol population:

$$\overline{\rho} = \sum [S_i], \tag{13}$$

and k_i is the imaginary index of refraction of the absorbing component in the parent particle. *Sokolik and Toon* [1999] compared the VWR method with an approximation referred to as the Bruggeman approximation. The Bruggeman approximation is derived from an integral equation for propagation of electromagnetic waves in inhomogeneous media and calculates the effective dielectric constant from the dielectric constants of the mixtures in a multicomponent particle. For a particle with 90% quartz and 10% hematite (percentages by mass), the imaginary index of refraction calculated with the Bruggeman approach differs by about 60% at 0.5 μm wavelength from the VWR method. *Sokolik and Toon* [1999] also compared the VWR method with the Bruggeman approach for the real index of refraction and found no significant difference. *Sokolik and Toon* [1999] do not explain the calculated difference between the two methods for the imaginary index of refraction. *Kalashnikova and Sokolik* [2004] used the Bruggeman approach to calculate complex index of refraction of Saharan and Asian dust. For the Laramie filter data the VWR method is initially used; then the imaginary index of refraction is corrected by applying the difference that *Sokolik and Toon* [1999] determined between the VWR method and the Bruggeman approximation.

[57] The physical constants used for the complex index of refraction calculation for the chemical species collected on the filters are given in Table 2. As mentioned earlier, the index of refraction determined with the TAOPC is a weighted average index of refraction over 0.3 to 0.7 μm. The imaginary index of refraction of hematite, k_H, is a strong function of wavelength. Hence, to compare index of refraction determined from particles collected on the filters with those from the TAOPC measurements, the weighted average imaginary index of refraction for hematite, $\overline{k_H}$, is calculated with equation (2) where $m(\lambda)$ is replaced with $k_H(\lambda)$. The wavelength-dependent imaginary index of refraction is taken from the study of *Sokolik and Toon* [1999].

[58] Table 3 shows the calculated average complex index of refraction for the three CCSEM size ranges, for the long duration average filter data from July 2005, 21–23 February 2006, and 16–26 February 2006, and from the TAOPC index of refraction determination. The average real index of refraction is lowest in the 2.5–10 μm size class where the fraction of CaO is low, while the real index of refraction for the other size classes and from the long duration filter data are similar. The index of refraction range determined with the TAOPC is also in good agreement with the values derived from the filter data, but it extends to a higher value when the particles are assumed to be spherical for the PNR approach, and when the non-spherical and spherical phase function ratio (δ) is assumed to be same at 40° and 74°. The average imaginary index of refraction is highest in the long duration filter data and CCSEM 2.5–10 μm size class due to the higher overall fraction of Fe_2O_3 than in the smallest CCSEM size classes (Table 2). The imaginary index of refraction determined with the TAOPC is between the ranges of values found with the filter data.

[59] The assumption that all chemical constituents in the particles on the filters are homogeneously distributed throughout the particles is not realistic. To check this, the average index of refraction was also calculated for each individual particle type from Table 2 and then the average index of refraction for the aerosol population was calculated by weighting each particle type index of refraction by the number of particles. The results compare closely with the mass weighted calculation of index of refraction described above. Thus while it is incorrect to assume that all chemical constituents on the filters are homogeneously distributed throughout the particles, such assumptions do provide reasonable results for average index of refraction calculations.

4.5. Comparison With Previous Estimates of the Complex Index of Refraction of Tropospheric Aerosol

[60] Typical values of the average real index of refraction, n, for a sample of mineral dust particles in the visible region

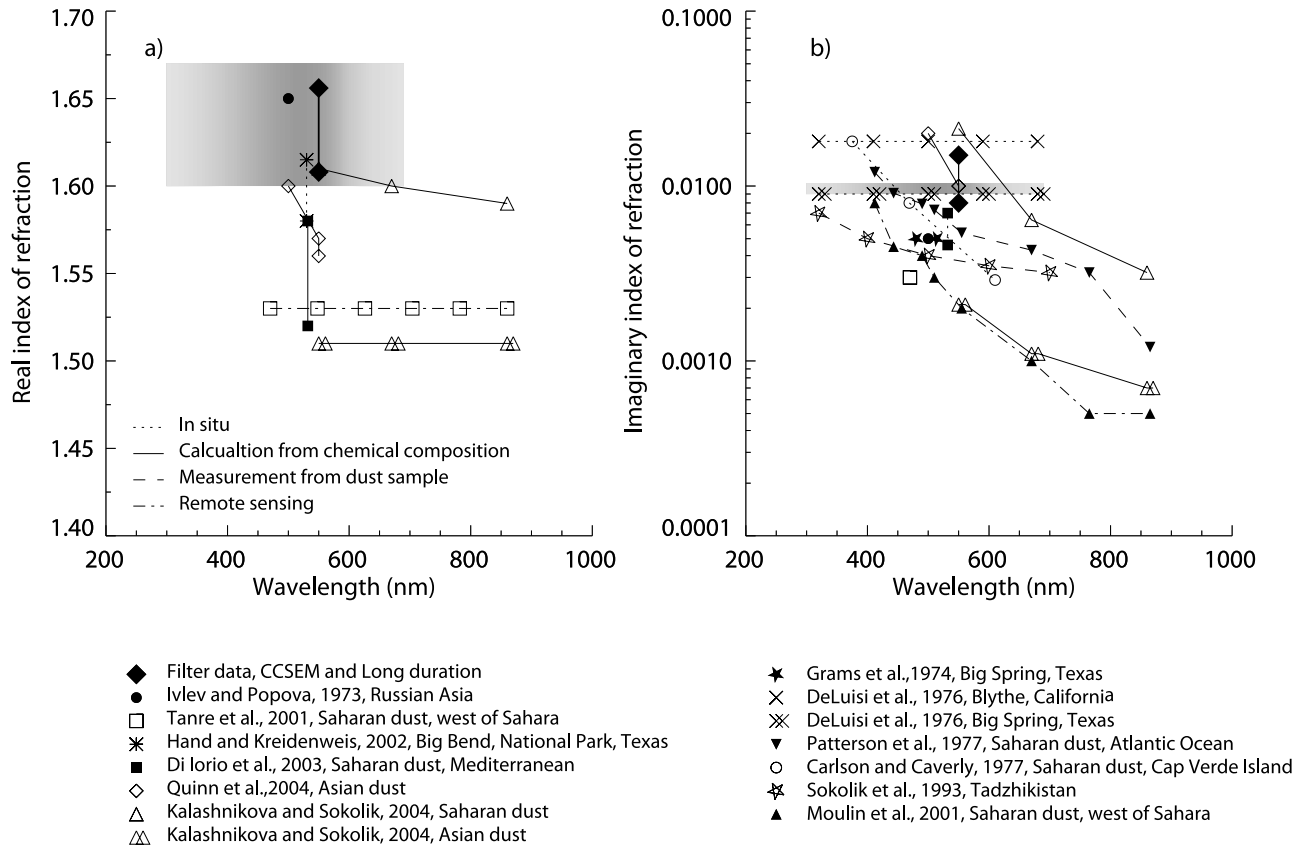

Figure 10. Real (a) and imaginary (b) indices of refraction determined in different studies. The lines between symbols indicate the technique used for index of refraction determination. For horizontal straight lines, an average between the first and last wavelength was given. For vertical straight lines, a variation of index of refraction at one wavelength was given. The locations of the measurements and the origin of the dust samples are also indicated. Grey-shaded areas show the refractive index determined with the TAOPC. The darker areas indicate that the determined index of refraction has a larger weight at these wavelengths. The filled diamonds shows the determination from the filter measurements.

vary from 1.50 to 1.65 [*Ivlev and Popova*, 1973; *Patterson et al.*, 1977; *Sokolik et al.*, 1993; *Tanre et al.*, 2001; *Hand and Kreidenweis*, 2002; *Di Iorio et al.*, 2003; *Kalashnikova and Sokolik*, 2004; *Quinn et al.*, 2004]. Figure 10a shows the spectrum of real indices of refraction determined in these various studies. Different techniques or types of measurements are used for the index of refraction determination (indicated with different types of lines in the figure): ground and space based remote sensing, *in situ* measurements, calculation based upon chemical composition from dust samples, and measurements of diffuse reflectance from dust samples. The chemical composition of dust particles varies with location [e.g., *Claquin et al.*, 1999; *Sokolik and Toon*, 1999], thus some of the difference in real index of refraction between the different studies arises from the source region of the dust particles. For example, *Kalashnikova and Sokolik* [2004] calculated a real index of refraction, at 0.5 μm, of 1.61 for typical Saharan dust and 1.51 for Asian dust.

[61] The average imaginary part, k, in the visible region for a sample of mineral dust particles is estimated to be in the range $5 \cdot 10^{-4}$–$3 \cdot 10^{-2}$ [*Grams et al.*, 1974; *Ivlev and Popova*, 1973; *DeLuisi et al.*, 1976a, 1976b; *Carlson and Caverly*, 1977; *Patterson et al.*, 1977; *Sokolik et al.*, 1993; *Tanre et al.*, 2001; *Di Iorio et al.*, 2003; *Kalashnikova and Sokolik*, 2004; *Quinn et al.*, 2004]. The imaginary index of refraction is a strong function of wavelength, with more absorption at shorter wavelengths and less absorption at longer wavelengths (see Figure 10b). Absorption by dust particles is mainly attributed to hematite (Fe_2O_3). Thus dust from regions with more hematite will have a higher imaginary index of refraction. Dust from the Sahara typically contains more hematite than dust from Asia [e.g., *Sokolik and Toon*, 1999]; *Claquin et al.* [1999] show that dust from the Sahel region (south of the Sahara) has even more hematite than the Sahara itself. In addition to the variation of index of refraction from different regions, *Tanre et al.* [2001] noted that imaginary indices of refraction determined from *in situ* measurement tend to be higher than determinations from the radiation field in the atmosphere (remote sensing).

[62] The gray shaded areas in Figure 10 indicate the real and imaginary index of refraction determined using the TAOPC from 2 hours of sampling in the winter in Laramie. The range in wavelength indicates the wavelength range over which the TAOPC indices of refraction are averaged, with the range of indices indicating the uncertainty of the measurement. The results from the filter data are also shown at a wavelength of 600 μm. Clearly the real index of

refraction determined by the TAOPC is above almost all previous estimates, but it is consistent with the filter analysis. The imaginary index of refraction is at the upper end of the range of previous measurements, as are the filter results. This comparison suggests that the TAOPC are reasonable for the aerosol sampled.

5. Summary and Conclusion

[63] A twin angle OPC was developed which measures forward scattering at 40° and 74°. This instrument is a modification of a single angle (40°) OPC which has been used for stratospheric aerosol measurements. The TAOPC was tested in the laboratory for index of refraction and size determination of spherical nonabsorbing particles having four different compositions (PSL, DEHS and Cargille index of refraction liquid AA 1.40 and A 1.51). Liquid monodisperse particles were generated and an Aerodynamic Particle Sizer was used for a size comparison. The index of refraction was determined for 55 distributions (including the two PSL distributions) and indicated that for monodisperse spherical particles >1.9 μm, the majority of the estimated indices of refraction with the TAOPC are between ±1% of the expected index of refraction. The index of refraction distributions are narrow and have relative uncertainties of 1 to 3% for the sizes investigated and the relative uncertainties decrease as size increases.

[64] Sizes determined with the TAOPC compare well with the reference size measurements, corrected for deformation of liquid particles, and since the derived indices of refraction are close to the expected values, the sizes determined with the TAOPC are assumed to approximate the true sizes of the particles. Also, the sizes of solid PSL particles determined with the TAOPC agree with the known sizes. Since the TAOPC measures scattering at two angles, the sizing of particles has a higher accuracy than sizing with a single angle OPC when index of refraction is not known, because the index of refraction does not have to be assumed.

[65] The measurement uncertainties of the TAOPC, determined using monodisperse particles, compare well with those determined using square wave pulses [*Miao*, 2001], indicating that statistical broadening in the PMT is the major source of uncertainties. The total sizing uncertainties at 40° are between 4 and 10% for particles >1.5 μm and between 5 and 15% at 74°. Non-uniform illumination and other uncertainty sources are minor contributors, as concluded by *Pinnick and Hofmann* [1973].

[66] Mineral dust particles >1 μm from a small urban mid-continental North American location were measured with the TAOPC and collected on different types of filters in February 2006. The average complex index of refraction was determined from measurements of the light scattering at two angles with the TAOPC and from calculations based upon chemical composition from a short duration filter, CCSEM analysis. They were also compared to those calculated from long duration (24–48 hours, and averages over 11 days) filters exposed at the same location during the same time period, and also previously, in July 2005. The sample average real index of refraction was determined to be in the range of 1.6 to 1.67, with values from the filter being at the lower end and values from the TAOPC spanning the range. The upper values from the TAOPC determination arise assuming spherical particles or that deviations in counter response due to non-spherical particles are the same at both angles. The lower values from the TAOPC determination arise when we assume that non-spherical particles create relative differences in the counter responses at 40° and 74° compared to the counter responses from spherical particles. The value from the CCSEM 2.5–10 μm size range was at the low end of the calculated range of values, because the sample contained less CaO. The imaginary index of refraction had a low value for the smallest size classes in the CCSEM analysis (1–2.5 μm) compared to the long duration filter data and to the CCSEM 2.5–10 μm size class due to less hematite in these samples. The TAOPC imaginary index of refraction was within the range of the values from the filter data.

[67] Compared to other studies (see Figure 10), the complex indices of refraction from this study are in the upper range, both for imaginary and especially for the real index of refraction. *Claquin et al.* [1999] show that the amount of hematite in dust in regions close to Laramie is relatively large and comparable to that of the Sahel region. Consequently, the imaginary index of refraction is expected to be relatively high.

[68] Modeling of the counter response ratio distribution of the TAOPC shows that the particles are non-spherical. This introduces uncertainties since the TAOPC data analysis assumes spherical particles so that Mie scattering theory can be used. This may affect the index of refraction determined from the TAOPC, depending on the relative deviations of the counter responses at 40° and 74° caused by non-sphericity. Although the derived real index of refraction is in the upper range of values from the literature, it spans the range of values obtained from the filter data. This suggests that the average index of refraction of coarse particles in Laramie is estimated reasonably well from the TAOPC measurements.

[69] Certainly questions can be raised about the usefulness of characterizing a complex mixture of atmospheric aerosol, which include non-spherical, absorbing, multicomponent, externally mixed particles, with a single complex index of refraction. Such a reduction is a significant simplification; however, such simplifications are required for many applications, including retrieving aerosol properties from in situ optical particle measurements [*Guyon et al.*, 2003; *Reidmiller et al.*, 2006; *Kuzmanoski et al.*, 2007] and active [*Ansmann et al.*, 2007; *Papayannis et al.*, 2007] and passive [*Remer et al.*, 2005; *Adamopoulos et al.*, 2007; *Mi et al.*, 2007; *Zieger et al.*, 2007] radiation measurements. Similar simplifications are required for completing radiative transfer calculations [*Kocifaj and Lukac*, 1998; *Caron et al.*, 2004] and to assess the role of aerosol in global climate models [*Ghan and Schwartz*, 2007]. Measurements such as reported here may provide useful additional constraints on the assumptions that are made for these various purposes when detailed knowledge of the atmospheric aerosol is not available.

[70] **Acknowledgments.** The instrument described here has been under intermittent development since the mid-1990s. The authors would like to acknowledge the effort of a number of individuals who helped bring these measurements to fruition. They are Lyle Womack, Jason Gonzales, Jim Hereford, Matt Burkhart, Lou King, Stan Smith, and Peter Liu. For the most recent support of this development, the authors acknowledge the US

National Science Foundation (OPP-023044, OPP-0538679, and ATM-0441836). The final measurements were most closely related to the ATM grant, although initially the instrument was developed under OPP support for polar stratospheric measurements.

References

Adamopoulos, A. D., H. D. Kambezidis, D. G. Kaskaoutis, and G. Giavis (2007), A study of aerosol particle sizes in the atmosphere of Athens, Greece, retrieved from solar spectral measurements, *Atmos. Res.*, *86*, 194–207.

Adriani, A., T. Deshler, G. DiDonfrancesco, and G. P. Gobbi (1995), Polar stratospheric clouds and volcanic aerosol during spring 1992 over McMurdo station, Antarctica: Lidar and particle counter comparisons, *J. Geophys. Res.*, *100*, 25,877–25,897.

Alfaro, S. C., S. Lafon, J. L. Rajot, P. Formenti, A. Gaudichet, and M. Maille (2004), Iron oxides and light absorption by pure desert dust: An experimental study, *J. Geophys. Res.*, *109*, D08208, doi:10.1029/2003JD004374.

Andreae, M. O., and A. Gelencser (2006), Black carbon or brown carbon? The nature of light-absorbing carbonaceous aerosols, *Atmos. Chem. Phys.*, *6*, 3131–3148.

Ansmann, A., U. Wandinger, O. Le Rille, D. Lajas, and A. G. Straume (2007), Particle backscatter and extinction profiling with the spaceborne high-spectral-resolution Doppler lidar ALADIN: Methodology and simulations, *Appl. Opt.*, *46*, 6606–6622.

Aptowicz, K. B., R. G. Pinnick, S. C. Hill, Y. L. Pan, and R. K. Chang (2006), Optical scattering patterns from single urban aerosol particles at Adelphi, Maryland, USA: A classification relating to particle morphologies, *J. Geophys. Res.*, *111*, D12212, doi:10.1029/2005JD006774.

Arimoto, R., W. Balsam, and C. Schloesslin (2002), Visible spectoscopy of aerosol particles collected on filters: Iron-oxide minerals, *Atmos. Environ.*, *36*, 89–96.

Baron, P. A., and K. Willeke (2001), *Aerosol Measurement: Principles, Techniques, and Applications*, xxiii, 1131 pp., Wiley-Interscience, New York.

Baron, P. A., G. Deye, A. Martinez, and E. Jones (2004), Apparent size shifts in measurements of droplets with the aerodynamic particle sizer and the aerosizer, *23rd Annual AAAR Meet.*

Baumgardner, D., J. E. Dye, B. Gandrud, K. Barr, K. Kelly, and K. R. Chan (1996), Refractive, indices of aerosols in the upper troposphere and lower stratosphere, *Geophys. Res. Lett.*, *23*, 749–752.

Berglund, R. N., and B. Y. H. Liu (1973), Generation of monodisperse aerosol standards, *Environ. Sci. Technol.*, *7*, 147–153.

Bond, T. C., and R. W. Bergstrom (2006), Light absorption by carbonaceous particles: An investigative review, *Aerosol. Sci. Tech.*, *40*, 27–67.

Carlson, T. N., and R. S. Caverly (1977), Radiative characteristics of Saharan dust at solar wavelengths, *J. Geophys. Res.*, *82*, 3141–3152.

Caron, J., C. Andraud, and J. Lafait (2004), Radiative transfer calculations in multilayer systems with smooth or rough interfaces, *J. Mod. Opt.*, *51*, 575–595.

Claquin, T., M. Schulz, and Y. J. Balkanski (1999), Modeling the mineralogy of atmospheric dust sources, *J. Geophys. Res.*, *104*, 22,243–22,256.

Clarke, A. D., et al. (2004), Size distributions and mixtures of dust and black carbon aerosol in Asian outflow: Physiochemistry and optical properties, *J. Geophys. Res.*, *109*, D15S09, doi:10.1029/2003JD004378.

DeLuisi, J. J., et al. (1976a), Results of a comprehensive atmospheric aerosol radiation experiment in southwestern United-States. 1: Size distribution, extinction optical depth and vertical profiles of aerosols suspended in atmosphere, *J. Appl. Meteorol.*, *15*, 441–454.

DeLuisi, J. J., et al. (1976b), Results of a comprehensive atmospheric aerosol radiation experiment in southwestern United-States. 2: Radiation flux measurements and theoretical interpretation, *J. Appl. Meteorol.*, *15*, 455–463.

Deshler, T., B. J. Johnson, D. J. Hofmann, and B. Nardi (1996), Correlations between ozone loss and volcanic aerosol at altitudes below 14 km over McMurdo Station, Antarctica, *Geophys. Res. Lett.*, *23*, 2931–2934.

Deshler, T., G. B. Liley, G. Bodeker, W. A. Metthews, and D. J. Hofmann (1997), Stratospheric aerosol following Pinatubo, comparison of the north and south mid latitudes using in situ measurements, *Adv. Space Res.*, *20*, 2057–2061.

Deshler, T., B. Nardi, A. Adriani, F. Cairo, G. Hansen, F. Fierli, A. Hauchecorne, and L. Pulvirenti (2000), Determining the index of refraction of polar stratospheric clouds above Andoya (69 degrees N) by combining size-resolved concentration and optical scattering measurements, *J. Geophys. Res.*, *105*, 3943–3953.

Deshler, T., M. E. Hervig, D. J. Hofmann, J. M. Rosen, and J. B. Liley (2003a), Thirty years of in situ stratospheric aerosol size distribution measurements from Laramie, Wyoming (41 degrees N), using balloon-borne instruments, *J. Geophys. Res.*, *108*(D5), 4167, doi:10.1029/2002JD002514.

Deshler, T., et al. (2003b), Large nitric acid particles at the top of an Arctic stratospheric cloud, *J. Geophys. Res.*, *108*(D16), 4517, doi:10.1029/2003JD003479.

Di Iorio, T., A. di Sarra, W. Junkermann, M. Cacciani, G. Fiocco, and D. Fua (2003), Tropospheric aerosols in the Mediterranean. 1: Microphysical and optical properties, *J. Geophys. Res.*, *108*(D10), 4316, doi:10.1029/2002JD002815.

Dick, W. D., P. H. McMurry, and J. R. Bottiger (1994), Size-dependent and composition-dependent response of the Dawn-A multiangle single-particle optical-detector, *Aerosol. Sci. Tech.*, *20*, 345–362.

Ghan, S. J., and S. E. Schwartz (2007), Aerosol properties and processes—A path from field and laboratory measurements to global climate models, *BAMS*, *88*, 1059, doi:10.1175/BAMS-88-7-1059.

Grams, G. W., I. H. Blifford, D. A. Gillette, and P. B. Russell (1974), Complex index of refraction of airborne soil particles, *J. Appl. Met.*, *13*, 459–471.

Guyon, P., B. Graham, J. Beck, O. Boucher, E. Gerasopoulos, O. L. Mayol-Bracero, G. C. Roberts, P. Artaxo, and M. O. Andreae (2003), Physical properties and concentration of aerosol particles over the Amazon tropical forest during background and biomass burning conditions, *Atmos. Chem. Phys.*, *3*, 951–967.

Han, Z. (1999), Characterization of the optical properties of continental aerosols during SWYVIS, M.S. thesis, Univ. of Wyoming, Laramie, Wyo.

Hand, J. L., and S. M. Kreidenweis (2002), A new method for retrieving particle refractive index and effective density from aerosol size distribution data, *Aerosol. Sci. Tech.*, *36*, 1012–1026.

Hasan, H., and T. G. Dzubay (1983), Apportioning light extinction coefficients to chemical-species in atmospheric aerosol, *Atmos. Environ.*, *17*, 1573–1581.

Hervig, M. E., T. Deshler, and J. M. Russell (1998), Aerosol size distributions obtained from HALOE spectral extinction measurements, *J. Geophys. Res.*, *103*, 1573–1583.

Hill, S. C., A. C. Hill, and P. W. Barber (1984), Light-scattering by size shape distributions of soil particles and spheroids, *Appl. Opt.*, *23*, 1025–1031.

Hofmann, D. J., and T. Deshler (1991), Stratospheric cloud observations during formation of the Antarctic ozone hole in 1989, *J. Geophys. Res.*, *96*, 2897–2912.

Hofmann, D. J., J. M. Rosen, T. J. Pepin, and R. G. Pinnick (1975), Stratospheric aerosol measurements. 1: Time variations at northern midlatitudes, *J. Atmos. Sci.*, *32*, 1446–1456.

Horvath, H. (1995), Size segregated light-absorption coefficient of the atmospheric aerosol, *Atmos. Environ.*, *29*, 875–883.

Hu, H. L., X. B. Li, Y. C. Zhang, and T. Li (2006), Determination of the refractive index and size distribution of aerosol from dual-scattering-angle optical particle counter measurements, *Appl. Opt.*, *45*, 3864–3870.

Ivlev, L. S., and S. I. Popova (1973), The complex refractive indices of substances in the atmospheric-aerosol dispersed phase, *Izv. Atmos. Oceanic Phys.*, *9*, 587–591.

Jaggard, D. L., C. Hill, R. W. Shorthill, D. Stuart, M. Glantz, F. Rosswog, B. Taggart, and S. Hammond (1981), Light-scattering from particles of regular and irregular shape, *Atmos. Environ.*, *15*, 2511–2519.

Kalashnikova, O. V., and I. N. Sokolik (2004), Modeling the radiative properties of nonspherical soil-derived mineral aerosols, *J. Quant. Spectrosc. Radiat. Transfer*, *87*, 137–166.

Kirchstetter, T. W., T. Novakov, and P. V. Hobbs (2004), Evidence that the spectral dependence of light absorption by aerosols is affected by organic carbon, *J. Geophys. Res.*, *109*, D21208, doi:10.1029/2004JD004999.

Kocifaj, M., and J. Lukac (1998), Using the multiple scattering theory for calculation of the radiation fluxes from experimental aerosol data, *J. Quant. Spectrosc. Radiat. Transfer*, *60*, 933–942.

Kuzmanoski, M., M. A. Box, B. Schmid, G. P. Box, J. Wang, P. B. Russell, D. Bates, H. H. Jonsson, E. J. Welton, and J. H. Seinfeld (2007), Aerosol properties computed from aircraft-based observations during the ACE-Asia campaign. 2: A case study of lidar ratio closure, *Aerosol. Sci. Tech.*, *41*, 231–243.

Lafon, S., I. N. Sokolik, J. L. Rajot, S. Caquineau, and A. Gaudichet (2006), Characterization of iron oxides in mineral dust aerosols: Implications for light absorption, *J. Geophys. Res.*, *111*, D21207, doi:10.1029/2005JD007016.

Liu, L., M. I. Mishchenko, J. W. Hovenier, H. Volten, and O. Munoz (2003), Scattering matrix of quartz aerosols: comparison and synthesis of laboratory and Lorenz-Mie results, *J. Quant. Spectrosc. Radiat. Transfer*, *79*, 911–920.

Ma, X., J. Q. Lu, R. S. Brock, K. M. Jacobs, P. Yang, and X. Hu (2003), Determination of complex refractive index of polystyrene microspheres from 370 to 1610 nm, *Phys. Med. Biol.*, *48*, 4165–4172.

Malm, W. C., J. F. Sisler, D. Huffman, R. A. Eldred, and T. A. Cahill (1994), Spatial and seasonal trends in particle concentration and optical extinction in the United-States, *J. Geophys. Res.*, *99*, 1347–1370.

Mi, W., Z. Q. Li, X. G. Xia, B. Holben, R. Levy, F. S. Zhao, H. B. Chen, and M. Cribb (2007), Evaluation of the moderate resolution imaging spectroradiometer aerosol products at two aerosol robotic network stations in China, *J. Geophys. Res.*, *112*, D22S08, doi:10.1029/2007JD008474.

Miao, Q. (2001), An analysis of errors associated with the in situ measurement of aerosol size and concentration with optical particle counters, M.S. thesis, Univ. of Wyoming, Laramie, Wyo.

Mie, G. (1908), Beiträge zur Optik trüber Medien, *Ann. Physik.*, *25*, 377–445.

Mishchenko, M. I., L. D. Travis, R. A. Kahn, and R. A. West (1997), Modeling phase functions for dustlike tropospheric aerosols using a shape mixture of randomly oriented polydisperse spheroids, *J. Geophys. Res.*, *102*, 16,831–16,847.

Ouimette, J. R., and R. C. Flagan (1982), The extinction coefficient of multicomponent aerosols, *Atmos. Environ.*, *16*, 2405–2419.

Palmer, K. F., and D. Williams (1975), Optical constants of sulfuric-acid application to clouds of Venus, *Appl. Opt.*, *14*, 208–219.

Papayannis, A., R. E. Mamouri, G. Chourdakis, G. Georgoussis, A. Amiridis, D. Paronis, G. Tsaknakis, and G. Avdikos (2007), Retrieval of the optical properties of tropospheric aerosols over Athens, Greece combining a 6-wavelength Raman-lidar and the CALIPSO VIS-NIR lidar system: Case-study analysis of a Saharan dust intrusion over the Eastern Mediterranean, *J. Optoelectron. Adv. Mater.*, *9*, 3514–3517.

Patterson, E. M., D. A. Gillette, and B. H. Stockton (1977), Complex index of refraction between 300 and 700 nm for Saharan aerosols, *J. Geophys. Res.*, *82*, 3153–3160.

Pinnick, R. G. (1972), Measured light scattering properties of individual aerosol particles compared to Mie scattering theory, Ph.D. thesis, Univ. of Wyoming, Laramie, Wyo.

Pinnick, R. G., and D. J. Hofmann (1973), Efficiency of light-scattering aerosol particle counters, *Appl. Opt.*, *12*, 2593–2597.

Pinnick, R. G., and J. M. Rosen (1979), Response of Knollenberg light-scattering counters to non-spherical doublet polystyrene latex aerosols, *J. Aerosol. Sci.*, *10*, 533–538.

Pinnick, R. G., D. E. Carroll, and D. J. Hofmann (1976), Polarized-light scattered from monodisperse randomly oriented nonspherical aerosol-particles—measurements, *Appl. Opt.*, *15*, 384–393.

Quinn, P. K., et al. (2004), Aerosol optical properties measured on board the Ronald H. Brown during ACE-Asia as a function of aerosol chemical composition and source region, *J. Geophys. Res.*, *109*, D19S01, doi:10.1029/2003JD004010.

Reid, J. S., et al. (2003), Comparison of size and morphological measurements of coarse mode dust particles from Africa, *J. Geophys. Res.*, *108*(D19), 8593, doi:10.1029/2002JD002485.

Reidmiller, D. R., P. V. Hobbs, and R. Kahn (2006), Aerosol optical properties and particle size distributions on the east coast of the united states derived from airborne in situ and remote sensing measurements, *J. Atmos. Sci.*, *63*, 785–814.

Remer, L. A., et al. (2005), The MODIS aerosol algorithm, products, and validation, *J. Atmos. Sci.*, *62*, 947–973.

Rosen, J. M. (1964), Vertical distribution of dust to 30 kilometers, *J. Geophys. Res.*, *69*, 4673–4676.

Shen, Z. X., J. J. Cao, X. Y. Zhang, R. Arimoto, J. F. Ji, W. L. Balsam, Y. Q. Wang, R. J. Zhang, and X. X. Li (2006), Spectroscopic analysis of iron-oxide minerals in aerosol particles from northern China, *Sci. Total Environ.*, *367*, 899–907.

Shi, Z. B., L. T. Shao, T. P. Jones, and S. L. Lu (2005), Microscopy and mineralogy of airborne particles collected during severe dust storm episodes in Beijing, China, *J. Geophys. Res.*, *110*, D01303, doi:10.1029/2004JD005073.

Sokolik, I. N., and O. B. Toon (1999), Incorporation of mineralogical composition into models of the radiative properties of mineral aerosol from UV to IR wavelengths, *J. Geophys. Res.*, *104*, 9423–9444.

Sokolik, I. N., A. Andronova, and T. C. Johnson (1993), Complex refractive index of atmospheric dust aerosols, *Atmos. Environ.*, *27*, 2495–2502.

Stelson, A. W. (1990), Urban aerosol refractive-index prediction by partial molar refraction approach, *Environ. Sci. Technol.*, *24*, 1676–1679.

Sugita, T., Y. Kondo, M. Koike, M. Kanada, N. Toriyama, H. Nakajima, T. Deshler, and R. Imasu (1999), Balloon-borne optical counter for in situ aerosol measurements, *J. Atmos. Chem.*, *32*, 183–204.

Szymanski, W. W., T. Ciach, A. Podgorski, and L. Gradon (2000), Optimized response characteristics of an optical particle spectrometer for size measurement of aerosols, *J. Quant. Spectrosc. Radiat. Transfer*, *64*, 75–86.

Tanre, D., Y. J. Kaufman, B. N. Holben, B. Chatenet, A. Karnieli, F. Lavenu, L. Blarel, O. Dubovik, L. A. Remer, and A. Smirnov (2001), Climatology of dust aerosol size distribution and optical properties derived from remotely sensed data in the solar spectrum, *J. Geophys. Res.*, *106*, 18,205–18,217.

TSI (2006), Model 3079 portable atomizer aerosol generator; revision c, Operational and service manual, TSI Inc., Minneapolis, Minn.

Weast, R. C., and M. J. Astle (Eds.) (1980), *Handbook of Chemistry and Physics 60th edition*, CRC Press, Inc, Boca Raton, Fla.

Weber, S., P. Hoffmann, J. Ensling, A. N. Dedik, S. Weinbruch, G. Miehe, P. Gutlich, and H. M. Ortner (2000), Characterization of iron compounds from urban and rural aerosol sources, *J. Aerosol. Sci.*, *31*, 987–997.

Willeke, K., and P. A. Baron (1993), *Aerosol Measurement: Principles, Techniques, and Applications*, xviii, 876 pp., Van Nostrand Reinhold, New York.

Zhao, F. S., Z. B. Gong, H. L. Hu, M. Tanaka, and T. Hayasaka (1997), Simultaneous determination of the aerosol complex index of refraction and size distribution from scattering measurements of polarized light, *Appl. Optics.*, *36*, 7992–8001.

Zieger, P., T. Ruhtz, R. Preusker, and J. Fischer (2007), Dual-aureole and sun spectrometer system for airborne measurements of aerosol optical properties, *Appl. Opt.*, *46*, 8542–8552.

T. Deshler and D. C. Montague, Department of Atmospheric Science, University of Wyoming, Laramie, WY 82071, USA.

T. Eidhammer, Department of Atmospheric Science, Colorado State University, Ft. Collins, CO 80523, USA. (trude@atmos.colostate.edu)